

Review

The “Expanded” Phases in the Low-Temperature Treated Stainless Steels: A Review

Francesca Borgioli 

Department of Industrial Engineering, University of Florence, Via S. Marta 3, 50139 Florence, Italy; francesca.borgioli@unifi.it; Tel.: +39-055-275-8734

Abstract: Low-temperature treatments have become a valuable method for improving the surface hardness of stainless steels, and thus their tribological properties, without impairing their corrosion resistance. By using treatment temperatures lower than those usually employed for nitriding or carburizing of low alloy steels or tool steels, it is possible to obtain a fairly fast (interstitial) diffusion of nitrogen and/or carbon atoms; on the contrary, the diffusion of substitutional atoms, as chromium atoms, has significantly slowed down, therefore the formation of chromium compounds is hindered, and corrosion resistance can be maintained. As a consequence, nitrogen and carbon atoms can be retained in solid solutions in an iron lattice well beyond their maximum solubility, and supersaturated solid solutions are produced. Depending on the iron lattice structure present in the stainless steel, the so-called “expanded austenite” or “S-phase”, “expanded ferrite”, and “expanded martensite” have been reported to be formed. This review summarizes the main studies on the characteristics and properties of these “expanded” phases and of the modified surface layers in which these phases form by using low-temperature treatments. A particular focus is on expanded martensite and expanded ferrite. Expanded austenite–S-phase is also discussed, with particular reference to the most recent studies.

Keywords: stainless steels; low-temperature treatments; nitriding; carburizing; expanded austenite; S-phase; expanded martensite; expanded ferrite; corrosion resistance; wear resistance



Citation: Borgioli, F. The “Expanded” Phases in the Low-Temperature Treated Stainless Steels: A Review. *Metals* **2022**, *12*, 331. <https://doi.org/10.3390/met12020331>

Academic Editor: Andre Paulo Tschiptschin

Received: 30 December 2021

Accepted: 11 February 2022

Published: 14 February 2022

Publisher’s Note: MDPI stays neutral with regard to jurisdictional claims in published maps and institutional affiliations.



Copyright: © 2022 by the author. Licensee MDPI, Basel, Switzerland. This article is an open access article distributed under the terms and conditions of the Creative Commons Attribution (CC BY) license (<https://creativecommons.org/licenses/by/4.0/>).

1. Introduction

Stainless steels are used for a wide variety of applications, from components for the chemical and power engineering industries to household utensils and kitchenware [1,2]. Their success is due to their resistance to general corrosion in many environments, owing to the thin, adherent, and self-healing chromium-rich oxide film, which forms on the steel surface in the presence of oxygen. A chromium (Cr) content of at least 10.5 wt.% is required for the formation of this protective oxide film [2]. The addition of Cr stabilizes the body-centered cubic (b.c.c.) structure of ferrite, so that the phase transformation of ferrite into the face-centered cubic (f.c.c.) structure of austenite does not occur when the Cr content is higher than ~14 wt.% [3]. When nickel (Ni) is added, the austenite phase field, the so-called γ -loop, is expanded, and the austenite becomes stable in a wide temperature range [4]. By changing the amounts of Cr and Ni, as well as the alloy elements able to stabilize ferrite, such as molybdenum (Mo), silicon (Si), niobium (Nb), titanium (Ti), or those able to stabilize austenite, such as carbon (C), nitrogen (N), manganese (Mn), ferrite, martensite, or austenite lattices and their related microstructures can be obtained. Due to the important effect of microstructure on their properties, stainless steels are usually classified according to their microstructure into five groups: ferritic, martensitic, austenitic, duplex (ferritic-austenitic), and precipitation hardening stainless steels [1,2].

Ferritic stainless steels are nonhardenable, ferromagnetic FeCr alloys, with a Cr content typically in the range of 10.5–30 wt.%, C up to ~0.2 wt.%, and with no or very little Ni. They are cheaper than austenitic CrNi grades, can have good ductility and formability, and are highly resistant to stress-corrosion-cracking, but they are subjected to ductile-to-brittle transition.

Martensitic stainless steels have Cr and C contents that are balanced so that the γ -loop is expanded, and austenite-to-martensite transformation can occur through quenching. Carbides may also be present in order to increase wear resistance. Cr is usually in the range of 10.5–18 wt.%, and C content may exceed 1.2 wt.%. High strength and hardness, as well as good toughness, can be attained through quenching and tempering heat treatments. A lower corrosion resistance is observed, in comparison with austenitic and ferritic grades.

Austenitic stainless steels have a fairly high content of austenite-stabilizing elements, such as Ni, Mn and N. Ni, with a content of 8 wt.% or higher, is the basis of CrNi AISI 300 series austenitic stainless steels, while it is partly substituted with Mn and N in CrMn AISI 200 series stainless steels. A negligible Ni amount, lower than 0.3 wt.%, is present in the so-called Ni-free stainless steels, in which Mn (9–24 wt.%) and N (0.45–1.1 wt.%) stabilize the austenite structure [5]. These steels are nonmagnetic, have excellent corrosion resistance, as well as ease of formability and weldability, and they can be employed from cryogenic to elevated temperatures.

Duplex stainless steels have a microstructure containing both ferrite and austenite. The amount of each phase is a function of the alloy element content, mainly of Cr and Ni, and heat treatment. These steels have a corrosion resistance comparable to that of austenitic stainless steels with a similar alloy element content, but they have a higher yield strength and improved resistance to stress–corrosion cracking and corrosion fatigue. Their toughness is between that of ferritic and austenitic stainless steels, but, as ferritic grades, they lack cryogenic toughness.

Precipitation hardening (PH) stainless steels contain, besides Cr and Ni, alloy elements, such as copper (Cu), aluminum (Al), and Ti, which allow them to harden by means of a solution and aging treatment. They are classified as martensitic, austenitic, and semi-austenitic, according to their microstructure after the solution-annealing heat treatment. Semi-austenitic steels transform into martensite during subsequent heat treatment. The formation of precipitates allows for high strength and maintaining a good corrosion resistance.

Modification of the surface characteristics of stainless steels may be needed in order to improve surface hardness, tribological properties, fatigue resistance, or resistance to localized corrosion in specific environments. Surface engineering techniques allow for overcoming the limitation of the different stainless steels grades by means of either coatings with hard compounds, obtained with processes as chemical vapor deposition (CVD), physical vapor deposition (PVD) and plasma spray, or through modifying the surface layers using diffusion processes [6]. Thermochemical processes, in which N and/or C surface alloying is performed by means of diffusion, are well known for the surface modification of low alloy and tool steels, and they have become an effective industrial practice. For low alloy and tool steels, nitriding is usually performed at temperatures in the range of 500–580 °C, and it produces modified surface layers consisting of an outer compound layer, in which Fe-based nitrides, γ -Fe₄N, and ϵ -Fe₂₋₃N, are present, and an inner diffusion layer, in which alloy element nitrides precipitates form in a N-rich ferrite matrix [7]. Carburizing is usually carried out at temperatures in the range of 850–950 °C, at which austenite is stable. After the carburizing step, quenching and tempering are performed, so that a C-rich martensite case can be produced [6].

When nitriding or carburizing treatments are applied to stainless steels using the same temperatures employed for low alloy and tool steels, hard Cr compounds (nitrides, carbides) are able to form, and the Cr-depleted matrix cannot maintain a uniform and protective passive film, therefore corrosion can easily occur [8,9]. The uptake of interstitial elements from the treatment atmosphere to the substrate is hindered by the passive layer, which acts as a diffusion barrier, so that a uniform treatment can be obtained only by previously removing or reducing this oxide layer [10–12]. These drawbacks of nitriding and carburizing can be overcome using the so-called low-temperature diffusion treatments. In fact, when the treatment temperature of nitriding or carburizing process is decreased, so that significant Cr (substitutional) diffusion is avoided while interstitial atoms can diffuse, in the so-called para-equilibrium conditions [13], it is possible to inhibit the formation of Cr

nitrides and carbides precipitates and obtain supersaturated solid solutions of the diffused interstitial atoms in austenite, ferrite, or martensite, which allow for a surface hardness increase without impairing the corrosion resistance.

The possibility of obtaining “expanded” phases by means of thermochemical treatments, performed at temperatures lower than those usually employed for nitriding and carburizing, was not recognized for many years. For austenitic stainless steels, the formation of a N-rich phase, which is now known as “expanded austenite” or “S-phase”, was reported in the mid-1980s, more or less in the same period, by different groups (Zhang and Bell [14,15], Ichii et al. [16,17], De Benedetti et al. [18–20], and Yasumaru and Kamachi [21], as recently reviewed in [11]), even if studies on nitriding at low temperatures date back to the 1970s [22,23]. Low-temperature carburizing dates back to 1983, when Kolster reported a process which was able to increase the fatigue and wear resistance of stainless steels, while maintaining the corrosion resistance [24]. This process was the basis of the proprietary treatment known as Kolsterizing. The possibility of applying low-temperature nitriding to martensitic and ferritic stainless steels has been neglected in consideration. In the same period, many studies reported nitriding treatments carried out at temperatures comparable to those used for low alloy steels, i.e., at temperature of 500 °C or higher [25–32]. Lower temperatures were used in a few studies, but the formation of “expanded” phases was hardly recognized [25,29,33]. The term “expanded martensite” was used in 2000 by Kim et al. [34] for the expanded phase observed in a nitrided AISI 420 martensitic stainless steel, while “expanded ferrite” was used later for the phase formed in treated martensitic [35], duplex [36], and ferritic stainless steels [37].

From the few studies reported in the 1980s, the interest for the characteristics of these expanded phases has grown, since the formation of these phases allows for high surface hardness, improved wear and fatigue resistance, and high corrosion resistance in chloride-ion (Cl^-) containing solutions. Until now, more than a thousand of papers have been published in academic journals, conference proceedings, and professional reports. Most part of the research papers, as well as of the brief overviews [38–45] and extended reviews [10–12,46–48], regarded the low-temperature treatments of austenitic stainless steels. Less attention has been paid to the other stainless steel types. Only few reviews reported the studies on expanded martensite and expanded ferrite [10,46,49]; however, an in-depth discussion of the studies on all the expanded phases is lacking.

The aim of the present review is to report the main studies on the formation, characteristics, and properties of the “expanded” phases obtained in stainless steels by using low-temperature treatments, and on the characteristics of the modified layers in which they form, with a particular focus on expanded martensite and expanded ferrite. The review is organized in four main sections. In the first section, the solid solutions of interstitial atoms in Fe phases and the formation of “expanded phases” are discussed. The second section regards expanded martensite, formed in martensitic and martensitic PH stainless steels, while the third section is devoted to expanded ferrite, formed in ferritic and duplex stainless steels. Finally, in the fourth section, expanded austenite–S-phase, formed in austenitic stainless steels, is discussed, with particular reference to the most recent studies.

2. N and C Solid Solutions in Fe Phases and Formation of “Expanded” Phases

N and C atoms are recognized as the most effective strengtheners of Fe-based solid solutions. According to phase diagrams, for pure Fe, the maximum solubility of N in b.c.c. α -Fe is 0.4 at.% at 592 °C, and in f.c.c., γ -Fe 10.3 at.% at 650 °C [50], while the maximum solubility of C in α -Fe is 0.104 at.% at 727 °C, and in γ -Fe 9.23 at.% at 1147 °C [51].

As reported by Gavriljuk [52], the N and C alloying in the f.c.c. phase influences the density of the electron states at Fermi level, causing different effects. When N atoms are in a solid solution in a f.c.c. Fe-based lattice, they increase the concentration of free electrons, having higher energy, and hence enhance the metallic character of the interatomic bonds, while C atoms promote the localization of electrons on the atomic sites. As a consequence, even if the atomic radius of N is smaller than that of C, the effective atom size of N atoms

in solid solution is larger, and thus a larger distortion of the f.c.c. lattice is produced. It should be noted that a similar effect on electron states was also observed for substitutional alloy elements, with elements located to the right of Fe in the periodic table, such as Ni, Cu, Si, and Al, which increase the concentration of free electrons in austenitic steels, while elements located to the left of Fe, such as Mn, Cr, and Mo, decrease it [53].

The influence of N and C atoms on the interatomic bonds leads to different atomic distribution in solid solutions. Using Mössbauer spectroscopy, it was shown that in the Fe–N solid solution, there is a tendency towards short-range ordering of N atoms, with the N atoms occupying two adjacent octahedral sites in 180° N–N pairs, as in the superstructure of γ' -Fe₄N, while in the Fe–C solid solution, there is a tendency towards clustering of C atoms [52]. N and C atoms also affect the distribution of substitutional solutes, with N promoting the distribution of substitutional atoms in austenite and C assisting the clustering of substitutional atoms [52]. Thus, it has been concluded that, in Fe-based solid solutions, alloy elements increasing the concentration of free electrons, such as N, Ni, Si, and Al, cause short range atomic ordering or a more homogeneous distribution of solute atoms, while atoms which promote the localization of electrons on atomic sites, such as C, Cr, Mn, and Mo, cause atomic clustering [52].

When martensite structure is taken into account, a similar behavior is observed, with N atoms having a tendency towards ordering and C atoms towards clustering [52].

The easy precipitation of Cr carbides can be considered a consequence of the clustering of C atoms and C-assisted clustering of Cr atoms. On the contrary, N atoms tend to shift the curve of the sensitization in the time-temperature-transformation diagram to the right on the time scale, and in the tempering of martensite they hinder the clustering of Cr atoms and precipitation of Cr nitrides. Thus, in an austenitic stainless steel, such as AISI 316, the C content is lower than 0.015 at.% in order to avoid carbide precipitation [54], while the equilibrium solubility of N in austenite is larger, even if fairly low, measuring less than 0.65 at.% [46].

In the “expanded” phases, the interstitial content can be several hundred times higher than the equilibrium solubility, causing a significant lattice expansion. According to phase diagrams, nitrides and carbides should be expected instead of interstitial solid solutions. From a thermodynamic perspective, the phase transition towards the corresponding nitrides and carbides is favorable enough for transition metals of lower groups, such as Ti, while for Fe nitrides and carbides, there is not a strong driving force towards compound formation [55,56], so N and C atoms can remain in solid solution in a Fe phase. Regarding Cr, it has a higher affinity to N and C in comparison with Fe, but the formation of Cr nitrides and carbides can be hindered by the use of low-temperature treatments. In fact, under these conditions, the diffusion of interstitial atoms such as N and C is several orders of magnitude higher than that of substitutional atoms (Cr, Mn, Mo, Ni), which are relatively “immobile” in the lattice [57], therefore, interstitial atoms tend to be retained in solid solutions, and the so-called “colossal” supersaturation [54,58] can occur.

As has been observed for interstitial solid solutions, the maximum N content in the expanded phases is higher than that of C. In the expanded austenite–S-phase, the maximum observed N content is ~38 at.% [58], also significantly beyond that of γ' -Fe₄N (19.3–20 at. % [50]), having a f.c.c. structure of metal atoms, while the maximum C content is ~19 at.% [59]. In expanded ferrite, obtained in ferritic stainless steels, a maximum N content of ~24 at.% was observed [60], and the reported maximum C content was ~10 at.% [61]. Similar values were detected in expanded martensite, with a maximum N content of ~22 at.% [62] and a maximum C content of ~10 at.% [63].

It should be noted that the large octahedral interstitial sites of the f.c.c. austenite phase allow for the accommodation of much more solute atoms (N and C) than the interstitial sites of the b.c.c. ferrite phase, therefore lower N and C contents were observed in expanded ferrite, and hence in expanded martensite. Thus, nitrides tend to precipitate more easily in ferrite and martensite than in austenite [46].

3. Expanded Martensite

The term “expanded martensite” can be ascribed to Kim et al. [34,64], who observed the presence of a martensitic phase with larger lattice parameters, in comparison with those of the bulk, in AISI 420 martensitic stainless steel samples nitrided at 350 and 400 °C. They named this phase by analogy with the designation “expanded austenite” for the phase observed in low-temperature nitrided austenitic stainless steels. Even if the term may seem odd, since martensite is already an expanded phase, and “expanded ferrite” has been observed to be a more appropriate name [65], it is widely used to indicate the phase that forms as an expansion of the original martensite phase in martensitic and martensitic PH stainless steels which have been nitrided and/or carburized at low temperatures. Similarly, the symbols $\alpha_{N'}$ and $\alpha_{C'}$ are used to indicate N- or C-rich expanded martensite phases, respectively.

The main characteristics of the modified surface layers containing expanded martensite, obtained by the nitriding or carburizing of martensitic and martensitic PH stainless steels, are summarized in Table 1.

Table 1. Main characteristics of the modified surface layers containing expanded martensite, obtained by the nitriding or carburizing of martensitic and martensitic PH stainless steels.

Properties		Nitriding	Carburizing
Formation temperature (without formation of Cr compounds) (°C)		200–350	200–450
Max. interstitial content in expanded martensite (at. %)		22	10
Max. surface hardness ($\text{kg}_f \text{mm}^{-2}$)	- expanded martensite only	1120	970
	- with Fe-based compounds	1560	1530
Hardness profile	- expanded martensite only	gradual change abrupt change	gradual change gradual change
	- with Fe-based compounds		
Load bearing capacity	- expanded martensite only	high	high
	- with Fe-based compounds	low	high
Dry sliding wear resistance		very good	good
Localized corrosion resistance	- expanded martensite only	good	good
	- with Fe-based compounds	variable ¹ /good ²	good

¹ Nitrides dispersed in expanded martensite. ² Nitrides forming a continuous outer layer.

3.1. Formation of Expanded Martensite

Expanded martensite has been reported to form in stainless steels which have a martensitic structure, i.e., martensitic [33,49,64–67] and martensitic PH [62,65,68–71] stainless steels.

In a martensite lattice, the diffusion of both interstitial and substitutional atoms is faster than that of the same atoms in f.c.c. austenite. As a consequence, modified surface layers are usually thicker than those produced in austenitic stainless steels using the same treatment conditions. Moreover, due to the low content or absence of Ni, which does not form nitrides and promotes the formation of a solid solution, the maximum treatment temperature to be used for avoiding the precipitation of nitrides and carbides, particularly Cr-based ones, is lower, and the treatment time is shorter than those used for austenitic stainless steels, especially for CrNi-based ones.

The phases present in the modified surface layers markedly depend on the treatment conditions, and, in particular, on the treatment temperature. For AISI 420 martensitic stainless steel, modified layers consisting of expanded martensite only were observed on samples which had been nitrided for 4 h at ultra-low temperatures, i.e., in the range of

200–300 °C [49]. When the treatment temperature was increased up to 400 °C, the h.c.p. ϵ -Fe_{2.3}N nitride was also formed, and when using temperatures higher than 400 °C, Cr nitride precipitates were present [49]. The early precipitation of Cr nitrides, such as that observed in Sandvik Nanoflex[®] (C 0.02 wt.%, Cr 12 wt.%, Ni 9 wt.%, Mo 4 wt.%, Cu 2 wt.%) PH stainless steel gas nitrided at 420 °C for 20 h, was ascribed to an energetically favorable orientation relationship between the expanded body centered tetragonal (b.c.t.) martensite lattice and NaCl-type CrN [69], analogous to the Baker–Nutting orientation relationship between the expanded α -Fe b.c.c. lattice and CrN [72], which lowered the nucleation barrier.

Nitriding at 450 °C or at higher temperatures caused the formation of an outer compound layer, in which both Cr and Fe nitrides were present [49,71,73,74]. Alphonsa et al. [30] observed the formation of an outer thin (2–5 μ m) layer consisting mainly of ϵ -Fe_{2.3}N with dispersed CrN on AISI 420 samples, nitrided at 530 °C for 20 h, while Dong et al. [71] reported the presence of CrN and γ' -Fe₄N in the modified layer formed on 17–4 PH stainless steel samples, which were plasma nitrided at temperatures in the range of 460–500 °C for 10 and 30 h.

The treatment atmosphere, and, in particular, the N₂ volume fraction and the addition of carburizing gas, also influences the phases that form in the modified layer. By increasing the N₂ content, the formation of nitrides was promoted, and the addition of CH₄ tended to favor the formation of ϵ -Fe_{2.3}(N,C) carbonitride [75]. For the plasma immersion ion implantation (PIII) process, the pulse voltage, and hence the energy of ion implantation, influenced the phases formed in the modified surface layers. On AISI 630 martensitic stainless steel, PIII nitriding caused the formation, in addition to the expanded martensite, of Fe₃N when high energy ion implantation at 25 kV was employed, and of Fe₄N when low energy, with 1.5 kV voltage, was used [76].

Regarding the carburizing treatment, when quenched AISI 420 martensitic stainless steel was carburized at 420 and 450 °C for 4 h [77], and at 400 °C for 8 h [78], Fe₃C was observed, together with C-rich expanded martensite.

Since the formation of Cr nitrides and carbides is related to diffusion phenomena, both treatment temperature and time are the process parameters which must be carefully controlled in order to avoid the formation of these precipitates. For martensitic stainless steels, the limit temperature for avoiding Cr nitride/carbide precipitation is considered to be ~350 °C for nitriding [10,79], ~400 °C for nitrocarburizing [79,80], and ~450 °C for carburizing [79,81], with a treatment duration of up to 8 h. When a treatment temperature of 400 °C was employed for AISI 420 martensitic stainless steel, 4 h was reported to be the threshold for sensitization, i.e., the precipitation of Cr compounds, for nitriding treatments [64,78], 6 h for nitrocarburizing [80], and more than 36 h for carburizing [82].

It was observed that, with nitrocarburizing treatments, thinner hardened layers were obtained as compared to those produced with nitriding at the same temperature and for the same treatment time [78,79,83], in contrast with the fact that C atoms diffuse faster than N atoms. As such, thicker hardened layers were expected for the nitrocarburized samples, as observed in austenitic stainless steels [84]. It has to be noted that, for the treatment conditions reported by Scheuer et al. [78,79] for the treatment of AISI 420 steel, in the modified layer, besides expanded martensite, ϵ -Fe_{2.3}N and ϵ -Fe_{2.3}(N,C) were also able to form in the outer part of the layer of nitrided and nitrocarburized samples, respectively. By comparing X-ray diffraction patterns, the volume fraction of ϵ -Fe_{2.3}(N,C) seemed higher than that of ϵ -Fe_{2.3}N, therefore it may be hypothesized that a slight thicker layer of carbonitride formed in nitrocarburized samples, in comparison with the nitride layer formed in nitrided steel. Taking into account that the diffusion rate of interstitial atoms is lower in nitride and nitrocarbide than in b.c.c. α -Fe [78], the apparently odd difference in the thickness of the hardened layers for the two treatments might be explained.

Taking advantage of the different diffusion rates of N and C atoms, and their possible interaction during the diffusion process, it was possible to delay the precipitation of Cr nitrides and/or carbides, and obtain modified layers consisting of expanded martensite

and Fe-based compounds by combining sequentially nitriding, nitrocarburizing, or carburizing [78]. The microstructure of the modified layer and hardness profile depended on the succession of secondary phases formation, which, in turn, depended on the sequence of thermochemical treatments.

Alloy composition influences the phases formed in the modified layer, and, in particular, the precipitation of CrN, and the thickness of modified layers, especially when low nitriding temperatures were used [60,85], therefore the maximum treatment temperature which allows the prevention of nitride and carbide precipitation depends on steel type [62].

The characteristics of the modified surface layers also depend on the previous heat treatment history of the steel. For martensitic stainless steels, low-temperature treatments are performed after quenching. Therefore, both tempering and surface treatment can be carried out in one step, or the surface treatment can be performed after the tempering step. Similar strategies can be employed for martensitic PH stainless steels, with the surface treatment and aging carried out as one step, or the surface treatment performed after aging.

The effect of previous heat treatment was reported by Figueroa et al. [86]. AISI 420 martensitic stainless samples were quenched and tempered at two different temperatures, 310 and 530 °C, for 1 h, and then they were PIII nitrided in the range of 340–500 °C. It was observed that the tempering temperature influenced the volume fraction of retained austenite, and that this phase, in turn, influenced the phases which formed during nitriding. Expanded austenite was able to form from the large amount of retained austenite present in the samples which were tempered at 310 °C, and by increasing the nitriding temperature up to 400 °C, it tended to become the prevailing phase, as compared to ϵ -nitride. In the samples which were tempered at 530 °C, containing a lower amount of retained austenite, ϵ -nitride formed when nitriding was performed at 360 °C. By increasing the treatment temperature to 430 °C, faster N diffusion tended to prevent the formation of ϵ -nitride, and expanded martensite, together with a low amount of CrN, precipitated at grain boundaries, was observed. It is interesting to note that, when nitriding was carried out at 475–500 °C, the modified layers of both sample types consisted of CrN precipitates in the ferrite matrix.

Nitriding and nitrocarburizing treatments allowed for the simultaneous aging step for PH steels [62,69,70,87]. Bottoli et al. [69] evaluated the effects of both the initial alloy microstructure and the low-temperature thermochemical treatment type on the surface and bulk properties of the Sandvik Nanoflex[®] PH stainless steel. By combining annealing and deformation treatments, it was possible to obtain a bulk material with different amounts of martensite and austenite. The characteristics of the modified surface layers obtained by means of nitriding or nitrocarburizing depended on the phases present in the alloy, as well as the hardening effect obtained by the aging of the bulk. Since N diffusivity is different in austenite and martensite, when both of these phases were present, inhomogeneous layers consisting of expanded austenite and expanded martensite were obtained. When martensite became the prevalent phase, an expanded martensite modified layer was obtained. When nitriding was performed at 420 °C (20 h), dark etched regions were present at grain boundaries, suggesting that Cr nitride precipitates were able to form, but when the nitriding temperature was reduced at 400 °C, Cr nitride precipitation was avoided. By using a nitrocarburizing atmosphere, the expanded martensite layer had a two-layer structure, with an outer N-rich zone and an inner C-rich one, as was observed for expanded austenite. When austenite was prevalent in the steel, the modified layer consisted of expanded austenite, and it was thinner than that consisting of expanded martensite obtained with the same nitriding conditions.

The possibility of performing the nitriding treatment after aging, or as a single treatment which allowed both nitriding and aging, was studied by Pinedo et al. [70] for a 17–4 PH stainless steel. Even if, for both strategies, modified surface layers consisting of expanded martensite were obtained with nitriding (400 °C, 20 h), a significantly thicker modified layer was produced in the solubilized and aged steel. It was hypothesized that the formation of the Cu-rich coherent precipitates, formed during aging, ensured that Cu did

not lower the N activity on martensite matrix during nitriding, contrary to what occurred in the solubilized only steel.

The shape of concentration profile of interstitial atoms as a function of depth, observed in the modified surface layers, depends on the phases that are able to form. When expanded martensite is the main phase and nitrides or expanded austenite are absent or in negligible amounts, the shape of N concentration profile vs. depth is very close to a complementary error function [87–90], suggesting a concentration independent diffusivity. When nitrides or expanded austenite form together with expanded martensite, the concentration profile is affected by the different diffusion rate in the different phases, and a trend with a fairly sharp decrease, a more or less wide plateau followed by a smoother decrease was observed [62,76].

The thermal stability of modified surface layers containing expanded martensite was studied by Baniyasi et al. [63] for carburized martensitic PH stainless steels. For carburized (450 °C, 18 h) 17–4 PH steel, the precipitation of Fe₃C was observed, beginning with heating at 200 °C for 2 h, while for 13–8Mo PH steel, carbide precipitation occurred during carburizing.

3.2. Characteristics of the Modified Surface Layers

The micrographs of the cross-section of AISI 420 martensitic stainless steel samples, which were plasma nitrided at 250 and 350 °C, are shown in Figure 1, together with the X-ray diffraction patterns of samples, untreated and treated in the range of 200–400 °C. The surface morphology and the microstructure of the cross-section of an AISI 431 martensitic stainless steel sample, plasma nitrided at 400 °C for 5 h, together with its X-ray diffraction patterns before and after the treatment, are depicted in Figure 2.

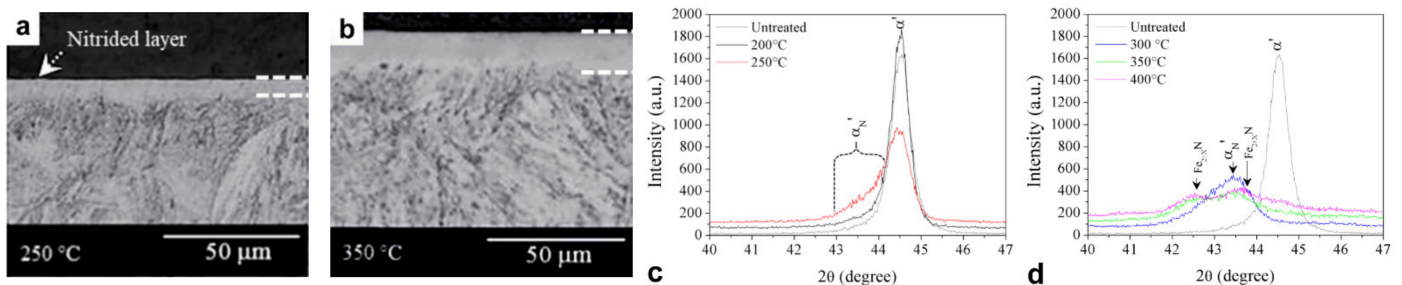


Figure 1. Micrographs of the cross-section of AISI 420 martensitic stainless steel samples plasma nitrided at 250 (a) and 350 (b) °C (etchant: Vilella’s reagent), and X-ray diffraction patterns of samples, untreated and nitrided at 200 and 250 °C (c), and in the range of 300–400 °C (d). (For further details, see ref. [49]). (Reprinted from *Materials Research Express*, 6 (2019), C.J. Scheuer et al., Ultra-low—to high-temperature plasma-assisted nitriding: revisiting and going further on the martensitic stainless steel treatment, 026529, ©IOP Publishing. Reproduced with permission. All rights reserved.)

The surface of low-temperature treated stainless steels with a martensite microstructure shows an etched appearance when plasma-based treatments are used, with the grains well delineated and reliefs at grain boundaries [66,70,83,91,92], as depicted in Figure 2a.

In nitrided samples, when Cr nitrides are not able to form, the cross-section microstructure of the outer part of the modified layer is almost featureless (Figure 1a,b). At a greater depth, the inner part of the modified layer becomes delineated by the chemical etching, and it does not show a strongly etched interface with the substrate. This characteristic was observed for modified layers consisting of expanded martensite only [49,68–71,89], and layers in which both expanded martensite and ϵ -Fe₂₋₃N nitride [49,67,93], or expanded martensite and expanded austenite [62,65,69], or expanded martensite, expanded austenite, and ϵ -Fe₂₋₃N [83] were detected. It should be noted that this featureless appearance may be due to the chemical etchings used, such as Marble’s reagent [33] or Vilella’s reagent [49,65,70,71,83], which are unable to etch Fe-based nitrides as well as N-rich phases, as was observed for the expanded austenite [11]. The microstructure of the modified layer can be better delin-

eated, highlighting the martensite structure, by using acetic glycergia [91], as showed in Figure 2b, or Kalling’s reagent [92].

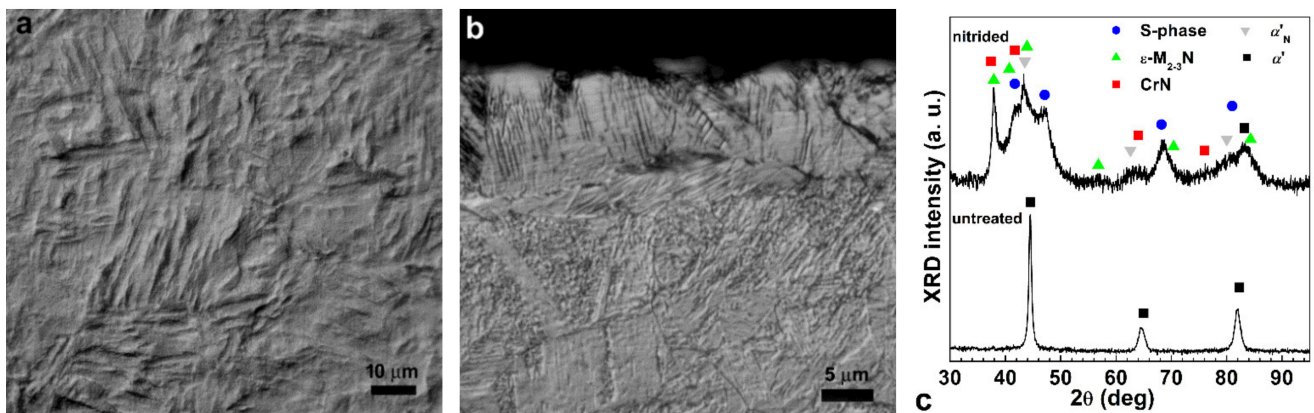


Figure 2. Surface morphology (a), cross-section micrograph (b) (etchant: glycergia) and X-ray diffraction patterns before and after the treatment (c) of an AISI 431 martensitic stainless steel sample plasma nitrided at 400 °C for 5 h. (For further experimental details, see ref. [91]).

The microstructure of the modified surface layers of nitrided samples depends on the formed phases and their volume fraction. When Fe-based nitrides are present in small amounts, they are not usually able to form a continuous layer. Acicular Fe-based nitrides precipitates were observed together with expanded martensite [66]. When the volume fraction of Fe nitrides increased, the formation of a double-layer structure was reported, with an outer compound layer consisting of nitrides and an inner diffusion layer, in which expanded martensite was present [94]. However, it should be noted that the featureless “white” part of the modified layer cannot be considered a compound layer, since it usually does not contain nitrides only. This part has a lower thickness in comparison with that of the whole hardened layer [78], thus it may be hypothesized that it is related to the N-richer part of the modified layer, consisting of Fe nitrides and N-rich expanded martensite and austenite, while the etched part of the layer is similar to the diffusion layer observed in low alloy steels. In nitrided samples, the “diffusion layer” is fairly thin, while it is thicker when nitrocarburizing treatment is performed [78]. In martensitic and martensitic PH stainless steels which are subjected to low-temperature nitriding, expanded austenite can form both from the retained austenite and as a consequence of the transformation of martensite in austenite due to the austenite stabilizing effect of N [83,86,95].

A fairly thin featureless layer, in which C-rich expanded martensite was present, with a thicker “diffusion layer”, was observed in carburized samples [77,78,82]. As an example, for AISI 420 martensitic stainless steel samples, which were quenched and then carburized at 450 °C for 4 h, Vilella’s reagent delineated a featureless “white” modified layer, which had a fairly low thickness (1.2–2.6 μm). By comparing the thickness of the modified layer with that of the hardened layer (about 55 μm), it was argued that C atoms diffused more deeply in the bulk than the etchant was able to reveal [77].

A different microstructure was observed when a large amount of expanded austenite was able to form. Using Kalling’s reagent, Frandsen et al. [62] showed that the modified layers of two PH stainless steels, Uddeholm Corrax[®] (C 0.03 wt.%, Cr 12 wt.% Ni, 9.2 wt.%, Mo 1.4 wt.%, Al 1.6 wt.%) and Sandvik Nanoflex[®], gas carburized at 508 °C, consisted of a two-layer microstructure, with an outer C-rich expanded austenite layer and an inner C-rich expanded martensite layer.

When C-rich expanded martensite formed, a martensite coarsening occurred, and plate-type martensite was present in the outer part of the modified layer [92]. This feature was observed in AISI 420 samples that were quenched and then carburized in the range of 350–450 °C for 12 h, and at 400 °C for times in the range of 12–36 h. The coarsening was related to the transformation from a predominantly lath-type martensite, present in

the as-hardened condition and characteristic of low C content, to plate-type martensite, characteristic of high C content. When higher treatment temperatures or longer durations were used, Cr-based carbides were able to form, thus a decrease in the C content in martensite occurred up to ferrite formation, and platelet refinement was observed, suggesting coarsening/refinement transformations.

Only a few studies have reported transmission electron microscopy (TEM) analysis of the modified layers. TEM analysis of the N-rich expanded martensite, formed in 17–4 PH stainless steel samples nitrided at 350 °C for 10 h, evidenced the presence of twins and slip lines across martensite laths [71]. Moreover, the selected area electron diffraction (SAED) patterns showed faint diffraction spots and streaks along $\langle 111 \rangle$ directions, suggesting the presence of high residual stress. In the same steel, nitrided at 440 °C for 8 h, stacking faults and dislocation groups were observed [68]. An interesting feature was observed in 15–5 PH and 17–7 PH stainless steels nitrided at 347 and 397 °C for 20 h [96,97]. TEM analysis evidenced the presence of plate-like structures, which had a lenticular shape, present in the martensite laths near the surface. These plates apparently grew from the surface, richer in N atoms, toward the bulk, and they were aligned along a few distinct orientations relative to the martensite laths. The analysis of SAED patterns suggested the formation of austenite, which was hypothesized to form as a consequence of a shear transformation, thus it was indicated as “martensitic austenite”.

The maximum nitrogen content in the expanded martensite depends on the treated stainless steels. In Sandvik Nanoflex® PH stainless steel nitrided at 425 °C, when using a nitriding potential $K_N = 2.37$ and a duration of 24 h in order to obtain a modified layer consisting of expanded martensite only, a N content as high as ~22 at.% was observed at the surface [62]. A maximum N content of ~20 at. % was registered in an AISI 431 martensitic stainless steel, subjected to ion implantation at 380 °C for 1 h at a voltage of 10 kV, [60], as well as in AISI 420, AISI 420C, and AISI 431 steels nitrided with the PIII process at 320 °C for 2 h [90]. A maximum C content of ~10 at.% was detected in 17–4 PH stainless steel carburized at 450 °C for 18 h [63].

When a high content of interstitial atoms is solubilized in martensite, as in the outer part of the modified layer, it may be hypothesized that the martensite lattice is distorted, and its tetragonality increases due to Zener ordering [98,99]. Under this condition, the interstitial atoms occupy the octahedral interstices of the ferrite lattice so that all the expanded $\langle 001 \rangle$ directions are parallel, forming a tetragonal structure. Evidence of the transition from a martensite having a more cubic structure, in which interstitial atoms occupy randomly all three sets of octahedral interstices in the three possible $\langle 001 \rangle$ directions, to an “ordered” tetragonal structure is given by the observed martensite coarsening in low-temperature carburized AISI 420 samples, from a lath-type martensite, related to the b.c.c. disordered structure, to a plate-type martensite, related to b.c.t. ordered structure [92]. A similar effect was not reported for nitrided samples, even if it may be hypothesized that it occurs, due to the similar microstructures reported for high-N and high-C martensites [100].

The evaluation of lattice tetragonality by means of X-ray diffraction analysis is complicated by the broadening of martensite peaks and their superposition with those of other phases. In the patterns of untreated martensitic or martensitic PH stainless steels, the tetragonality of the lattice is low, thus the peaks of a b.c.t. structure are usually indistinguishable from the peaks of a b.c.c. structure, even if the steel has a fairly high C content (see, for example, [101]). When N or C atoms are solubilized in the martensite structure, as a consequence of low-temperature treatment, a “tail” at lower diffraction angles is observed [33,60,69,77,94], thus an expansion of the lattice is hypothesized. The distinct shift of the peaks towards lower angles was reported as the interstitial content increases, hence the lattice expansion [64,69,70,77,102], even if it was not so marked as that observable for expanded austenite [103]. A broadening of the peaks was also registered [64,69,77,94]. The broadening of the peaks may be so marked, and Sun and Bell [89] hypothesized the formation of an amorphous phase in the modified layers of nitrided 17–4 PH steel. Frandsen et al. [62] observed a splitting of the peaks in the nitrided Ud-

deholm Corrax[®] and Sandvik Nanoflex[®] PH stainless steels, which was ascribed to the tetragonal distortion of the b.c.c. lattice to b.c.t., while only a broadening was registered for carburized Nanoflex[®] samples, which was similarly interpreted as due to a tetragonal distortion. Manova et al. [60] observed an anisotropic lattice expansion normal to the surface up to 3.5%, generally larger for the (110) planes than for the (200) planes, in martensitic and martensitic PH stainless steels which were subjected to nitrogen ion implantation at 380 °C for durations up to 3 h. On the contrary, Luiz et al. [104] observed an increase of 4.18% for the lattice parameter calculated for the (200) plane, while only of 2.10% for the lattice parameter calculated for the (110) plane, when the expanded martensite formed in nitrided UNS S41426 super-martensitic stainless steel was analyzed. On the basis of the analysis of X-ray diffraction patterns, SAED patterns and high resolution TEM (HRTEM) images of nitrided and carburized 15–5 PH stainless steel, Zangiabadi [96] reported that a high tetragonality occurred for N-rich expanded martensite, while it was smaller for C-rich expanded martensite.

3.3. Hardness of the Modified Surface Layers

The solubilization of further interstitial atoms in the martensite lattice causes an increase of surface hardness. The reported data often are also influenced by the presence of nitrides and/or carbides, that form together with expanded martensite, as well as by the hardness profiles. Regarding the expanded martensite only, values of 11 GPa ($\sim 1120 \text{ kg}_f \text{ mm}^{-2}$) were registered on nitrided samples through the nanoindentation technique [49]. The precipitation of ϵ -nitride in the expanded martensite caused a further increase of surface hardness, and values of 13.7 GPa ($\sim 1400 \text{ kg}_f \text{ mm}^{-2}$) were detected [49], while with a more continuous outer ϵ -nitride layer, values of $\sim 1560 \text{ kg}_f \text{ mm}^{-2}$ were registered [104]. When a fairly high amount of Cr nitrides was able to form, values as high as 1700–2000 $\text{kg}_f \text{ mm}^{-2}$ were reported [102]. Typical surface hardness for carburized samples was $\sim 970 \text{ kg}_f \text{ mm}^{-2}$ [81], but values up to $\sim 15 \text{ GPa}$ ($\sim 1530 \text{ kg}_f \text{ mm}^{-2}$), measured using nanoindentation techniques and probably also due to the strengthening effect of carbides precipitates, were registered [105]. The hardness profiles depended on the treatment conditions, and thus on the modified layer microstructure, as shown in Figure 3. When expanded martensite is able to form without relevant amounts of nitrides, as when fairly low nitriding temperatures are used (as 200–350 °C in Figure 3b), the hardness profile is smooth [49,67]. As high volume fractions of nitrides, and, in particular, Cr nitrides, are able to form (as for nitriding temperatures in the range 450–600 °C in Figure 3a), a thick hardened layer is observed, with values as high as $\sim 1400 \text{ kg}_f \text{ mm}^{-2}$ [49], followed by a region having a steep hardness decrease [30,49,74,106,107]. For carburized samples, fairly smooth hardness profiles are usually observed [81,107].

3.4. Tribological Properties of the Modified Surface Layers

The tribological properties of low-temperature treated martensitic and martensitic PH stainless steels depend on the phases formed in the modified surface layers and on the test conditions.

An improvement of wear resistance was reported for AISI 420 and AISI 431 martensitic stainless steels, which were subjected to N-ion implantation at temperatures in the range of 320–380 °C so that expanded martensite modified layers were able to form, when they were tested in ball-on-disc configuration against an alumina ball [88,90]. A significant wear reduction was observed also for AISI 630 martensitic stainless steel samples, nitrided and nitrocarburized by means of PIII process at 380 °C for 3 h, when they were tested using an oscillating ball-on-disc tribometer in unlubricated conditions against a tungsten carbide ball, and a reduction of the friction coefficient from approximately 0.8, for the untreated steel, to about 0.4, for the nitrided samples, was reported [76].

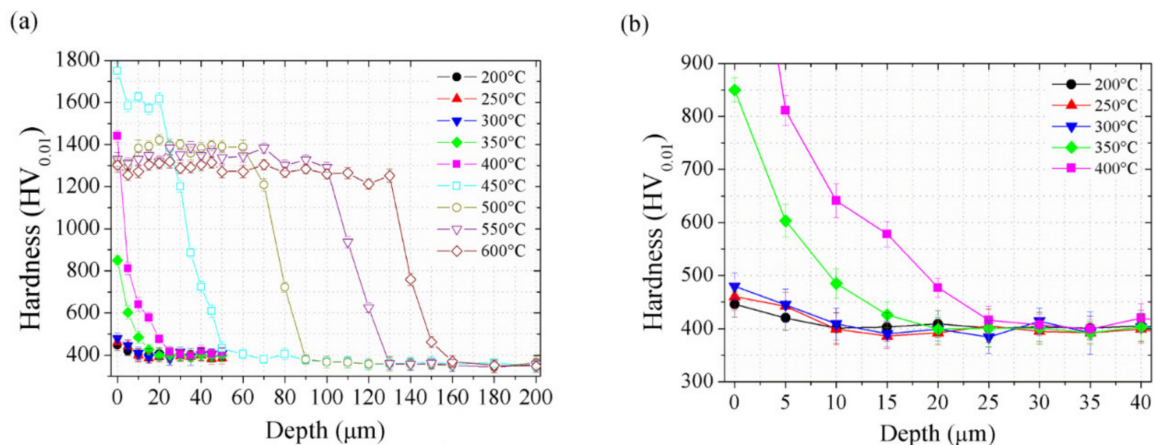


Figure 3. Microhardness profiles of AISI 420 martensitic stainless steel samples plasma nitrided in the range of 200–600 °C (a) and in the range of 200–400 °C (b). (For further details, see ref. [49]). (Reprinted from *Materials Research Express*, 6 (2019), C.J. Scheuer et al., Ultra-low—to high-temperature plasma-assisted nitriding: revisiting and going further on the martensitic stainless steel treatment, 026529, ©IOP Publishing. Reproduced with permission. All rights reserved.).

The wear resistance of martensitic 17–4 PH stainless steel, tested in unlubricated block-on-ring conditions with an AISI 52100 steel ring as counterface, was substantially improved when a modified layer consisting mainly of expanded martensite was obtained by means of plasma nitriding at 350 °C for 4 h [68].

The evaluation of the scratch resistance of a Fe-13Cr-3Ni-Mo martensitic stainless steel, subjected to nitriding and carburizing at temperatures in the range of 300–400 °C, evidenced that the scratch resistance was influenced by the different characteristics of the obtained modified surface layers [107]. In the nitrided samples, the modified layers consisted of N-rich expanded martensite and hard but brittle Fe-based nitrides, which allowed to have higher surface hardness and a low friction coefficient, but caused a micro-cutting predominance of the wear phenomena and many tensile cracks at the surface when a 15 N load was used. The carburized samples, having modified layers consisting of C-rich expanded martensite and small amounts of carbides, showed smoother microhardness profiles, which allowed a high load-bearing capacity, therefore, micro-ploughing was the predominant wear mechanism, and semi-circular cracks were observed for the 15 N load. The lower load-bearing capacity of modified layers consisting of an outer nitride-rich layer was observed also for micrometric-size protrusions, formed by sputter etching on AISI 420 martensitic stainless steel and then subjected to nitriding [108]. A significantly higher load-bearing capacity and scratch resistance of these protrusions was observed when nitriding produced modified surface layers, consisting mainly of expanded martensite and only a reduced amount of nitrides.

Similarly, the improvement of cavitation erosion resistance was reduced when Fe nitrides precipitates formed on the top of the modified surface layer of a plasma-nitrided AISI 410 martensitic stainless steel, allowing the detachment of entire grains due to shock-wave impact over the surface. However, when the removal of the outermost nitride-rich regions was performed, a marked decrease of the cavitation damage and erosion rate was observed [66]. The reduction of Fe nitrides precipitates and their decrease to nanometer size, such as those obtained using an active screen nitriding process, allowed the expanded martensite layer to markedly improve cavitation erosion resistance [67].

Modified surface layers consisting of expanded martensite and ϵ -nitride, such as those formed on an AISI 420 martensitic stainless steel plasma nitrided at 380 °C for 15 h, were able to improve the resistance to erosion and erosion corrosion, using neutral and acid slurries [109].

The precipitation of large volume fraction of hard nitrides is able to improve wear resistance in dry sliding conditions, in comparison with the untreated steels [27,74,110].

3.5. Corrosion Behavior of the Modified Surface Layers

When Cr is retained in solid solution, a protective surface oxide layer is maintained, and a good corrosion resistance is achieved. The further addition of N and/or C can improve the corrosion resistance, especially in Cl^- -containing solutions. As a matter of fact, all of the different phases that form as a consequence of low-temperature nitriding (expanded martensite, expanded austenite, Fe-based nitrides, Cr-based nitrides) contribute to the corrosion behavior. In the modified surface layers produced on martensitic and martensitic PH stainless steels, expanded martensite may be present together with other phases (Fe nitrides, expanded austenite), thus the evaluations of the corrosion behavior of expanded martensite alone are very limited. N-rich expanded martensite with a very small amount of γ' - Fe_4N nitride showed a good corrosion resistance in NaCl solution and reduction of pitting phenomena [94] (Figure 4), as well as C-rich expanded martensite [82]. An improved corrosion resistance in NaCl solutions was obtained when ε - Fe_{2-3}N nitride was able to form a continuous layer at the surface [74,86,93,106], or when ε -nitride formed together with expanded austenite [86], therefore both an increase in corrosion and pitting potential and a decrease in anodic current density were registered. When a multiphase structure was formed, such as expanded martensite with expanded austenite and/or ε -nitride, different behaviors were reported, with an increase [83,91,111] or slight decrease [65] in corrosion resistance. The study of Luiz et al. [104] on the corrosion behavior of PIII-nitrided UNS S41426 super-martensitic stainless steel showed that the modified layer consisting of expanded martensite and ε and γ' Fe-based nitrides was efficient in significantly improving the stability of the passive film for up to 30 days of immersion in 3.5% NaCl solution. When cyclic voltammetry tests were performed in 3.5% NaCl, the nitrided samples showed an enhanced resistance to passive film breakdown, in comparison with the untreated steel. However, instead of the typical localized corrosion phenomena, uniform corrosion of the nitrided layer was predominant, presumably due to the high content of Fe-based nitrides at the surface.

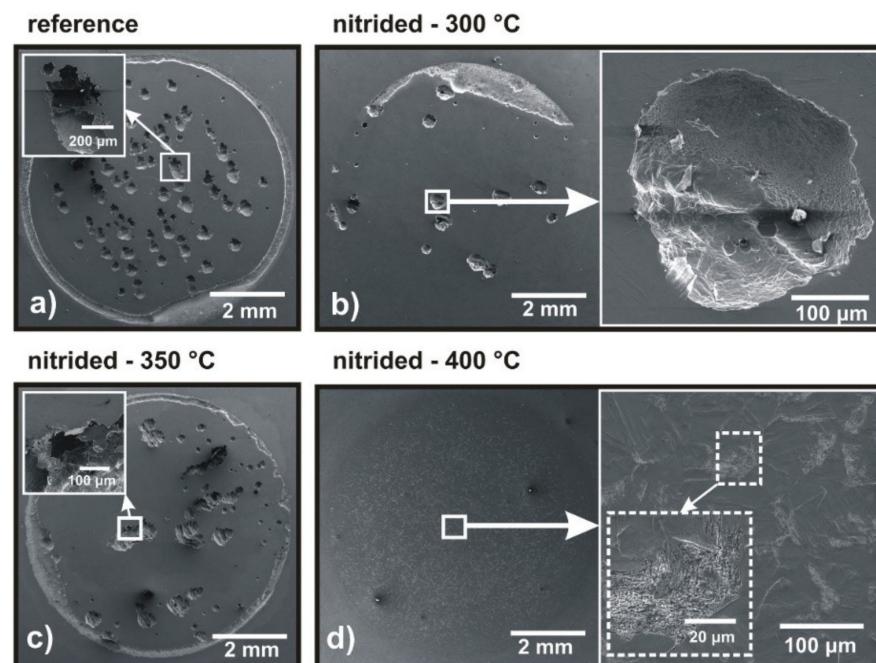


Figure 4. Surface microstructure of UNS S41426 super-martensitic stainless steel untreated (reference) (a) and nitrided at 300 (b), 350 (c), and 400 (d) °C, after corrosion tests in 3.5% NaCl. (For further details, see ref. [94]). (Reprinted from *Surface & Coatings Technology*, 351, B.C.E.S. Kurelo et al., Performance of nitrogen ion-implanted supermartensitic stainless steel in chlorine- and hydrogen-rich environments, 29–41, Copyright (2018), with permission from Elsevier).

The precipitation of fairly large volume fractions of Cr nitrides caused, as expected, a marked decrease in corrosion resistance [83,86]. Only when a thick compound layer consisting of nitrides was able to form, was higher corrosion resistance observed, such as for the AISI 410 martensitic stainless steel samples, which were plasma-nitrided in the range of 420–500 °C for 20 h and tested in 3.5% NaCl solution and 1% HCl acidic water solution [106].

4. Expanded Ferrite

The term “expanded ferrite” was initially used to indicate the phase that forms together with CrN when expanded austenite decomposes [112], or as a designation of “expanded martensite” [35,64,65]. Only since the mid-2000s was it used to indicate the interstitial-rich phase that forms in FeCr ferritic alloys [37] and duplex stainless steels [36]. The symbols α_N and α_C are also used to indicate N- or C-rich expanded ferrite phases.

Expanded ferrite has been observed to form in ferritic and duplex stainless steels subjected to low-temperature treatments.

4.1. Ferritic Stainless Steels

The main characteristics of the modified surface layers containing expanded ferrite, obtained by the nitriding or carburizing of ferritic stainless steels, are reported in Table 2.

Table 2. Main characteristics of the modified surface layers containing expanded ferrite, obtained by the nitriding or carburizing of ferritic stainless steels.

Properties		Nitriding	Carburizing
Formation temperature (without formation of Cr compounds) (°C)		<380	<470
Max. interstitial content in expanded ferrite (at. %)		24	10
Max. surface hardness ($\text{kg}_f \text{mm}^{-2}$)	- expanded ferrite only	1090	1000
	- with Fe-based compounds	1200	-
Hardness profile	- expanded ferrite only	gradual change	gradual change
	- with Fe-based compounds	abrupt change	-
Dry sliding wear resistance		good	-
Localized corrosion resistance	- expanded ferrite only	good	good
	- with Fe-based compounds	variable ¹ /good ²	-

¹ Nitrides dispersed in expanded ferrite. ² Nitrides forming a continuous outer layer.

4.1.1. Formation of Expanded Ferrite

In the ferritic stainless steels, the formation of a supersaturated solid solution of interstitial atoms in the b.c.c. lattice is reported [113–115], but it is competitive with that of the $\epsilon\text{-Fe}_{2.3}\text{N}$ nitride, which tends to form a continuous outer layer [116–120]. It is interesting to note that at low treatment temperatures the presence of $\gamma\text{-Fe}_4\text{N}$ is not usually reported, as well as that of a more or less expanded austenite, which should be stabilized by N or C atoms. The formation of expanded austenite was observed in a super-ferritic stainless steel, containing 28.12 wt.% Cr, 3.91 wt.% Ni, 2.44 wt.% Mo, which was subjected to N ion implantation at 100 °C at a lower implantation dose, whereas using higher implantation dose and energy N-rich martensite, together with Fe and Cr nitrides, formed [121]. It may be hypothesized that expanded austenite formation was promoted by the presence of Ni in the steel. The presence of expanded austenite was also reported in X10CrAl18 steel, which was nitrided with the PIII process at 300 °C for 3 h [122]. The Fe-based nitrides $\epsilon\text{-Fe}_{2.3}\text{N}$ and $\gamma\text{-Fe}_4\text{N}$ were observed, together with CrN, in ferritic stainless steels nitrided at temperatures typical of the nitriding of low alloy steels [31,114,116,123].

A continuous layer of expanded ferrite was observed by Kurelo et al. [113] on a UNS S44400 super-ferritic stainless steel subjected to nitriding by means of PIII process at temperatures in the range of 300–400 °C for 3 h. The presence of Fe nitride precipitates was assumed for the samples nitrided at 350 and 400 °C, even if clear peaks of these phases were not observed in X-ray diffraction patterns. Alphonsa et al. [114] reported the formation of expanded ferrite when AISI 430F steel was plasma nitrided at 380 °C (4 h, 80% N₂ + 20% H₂), while plasma nitrocarburizing (4 h, 78% N₂ + 20% H₂ + 2% C₂H₂) at the same temperature caused the formation of Fe₃N (or, more likely, the ε-Fe₂₋₃(N,C) carbonitride), together with a N- and C-rich expanded ferrite. With a treatment temperature of 400 °C, Fe₃N was present in both nitrided and nitrocarburized samples (probably, Fe₂₋₃(N,C) in nitrocarburized samples), and a further increase of the treatment temperature caused the formation of Cr nitrides in all the samples and of Fe and Cr carbides in the nitrocarburized ones. Modified surface layers of nitrided samples were thicker than those of samples nitrocarburized at the same temperature, similar to what was observed for martensitic stainless steels. Again, X-ray diffraction analysis suggests that the volume fraction of nitride in nitrided samples was lower than that of carbonitride in nitrocarburized samples, so that it may be hypothesized that the thickness of the modified layers was influenced by the slower diffusion of interstitial atoms in nitride/carbonitride [78]. De Sousa et al. [115] observed the formation of a thin, uniform layer consisting mainly of expanded ferrite on AISI 409 steel subjected to cathodic-cage nitrocarburizing at 400 °C for 5 h with a 95% N₂ + 5% CH₄ gas mixture, while for a plasma nitrocarburizing treatment, performed at the same temperature but for 10 h with a 78% H₂ + 20% N₂ + 2% CH₄ gas mixture, the formation of a significant amount of carbides and nitrides could also be inferred. Regarding carburizing treatments, C-rich expanded ferrite layer with a small volume fraction of carbides was reported to form on a E-BRITE stainless steel (Cr 25.8 wt.%, Ni 0.11 wt.%, Mo 0.99 wt.%) using a treatment temperature of 470 °C [61].

The reported studies put in light that the formation of expanded ferrite with none or a small amount of Fe-based nitrides is dependent on both treatment conditions and steel composition. Treatment temperature should be low enough to reduce the diffusivity of substitutional atoms, in particular of Cr atoms. N atoms inlet in the material should be reduced to prevent or reduce the formation of nitrides, but, at the same time, taking into account the high N atom diffusivity in ferrite, the amount of N inlet cannot be too low, in order to allow to form expanded ferrite. Since the formation of Cr-based compounds is both a chemical and diffusion driven process, not only the treatment temperature but also the duration must be taken into account. For nitriding and nitrocarburizing treatments, temperatures lower than 450 °C should be employed, in order to avoid Cr nitride precipitates [114]. However, by nitriding at 400 °C, the formation of Cr nitrides was avoided when the treatment time lasted for up to 4 h [113,114], but the formation occurred when a 20-h duration was used [124]. Similarly, with a 380°C nitriding temperature Cr nitride was not detected performing the treatment for 28 h, while the presence of this compound could not be excluded when the treatment time was 40 h [116]. Regarding carburizing, according to the study of Michal et al. [61], temperatures lower than 470 °C should be used to avoid carbide precipitation.

The shape of the concentration profile for N- and C-rich expanded ferrite was similar [60,61], and it was approximately that of a complementary error function, thus it was hypothesized that the diffusion coefficient of interstitial atoms in ferrite has a minimum dependence on concentration [61].

4.1.2. Characteristics of the Modified Surface Layers

The surface of low-temperature nitrided ferritic stainless steels has a slightly etched appearance, with grains well delineated, and small reliefs present at grain boundaries [125].

The cross-section microstructure of the modified surface layer containing expanded ferrite is almost featureless, as a consequence of the higher corrosion resistance of this layer in comparison with that of the substrate [61,113,114,125]. Below this layer, in the

region in which the N concentration decreased considerably, Kurelo et al. [113] observed needle-like structures, which were supposed to be related to the precipitation of γ' -Fe₄N nitride (Figure 5). Larisch et al. [116] reported that, when ϵ -Fe₂₋₃N nitride formed together with expanded ferrite, no sharp boundary with the substrate was delineated by chemical etching, and a peculiar microstructure was observed, with a “white” unetched outer zone which became progressively less “white” and containing needle-like structures, interpreted as deformation bands instead of γ' -Fe₄N precipitates. The comparison of the thickness of the unetched layer with that of the hardened layer suggests that diffusion of N atoms extends far beyond the fairly thin unetched zone [113], as was observed for martensitic stainless steels. Thus, it may be hypothesized that, in the unetched layer, N-rich expanded ferrite is present, eventually coming together with Fe-based nitrides, while a “diffusion” zone with a lower N-content extends below this layer. On the contrary, when carburizing was performed, comparable thicknesses were reported for the unetched layer and the hardened one [61].

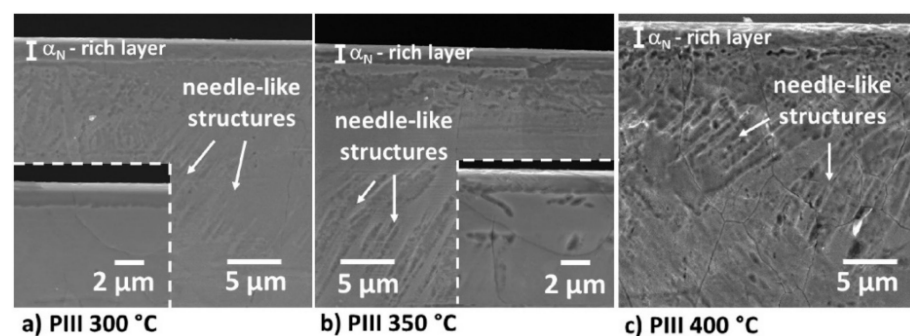


Figure 5. SEM micrographs of the cross-sections of UNS S44400 super-ferritic stainless steel samples PIII nitrided at 300 (a), 350 (b) and 400 (c) °C (etchant: Murakami’s reagent) (α_N : expanded ferrite). (For further details, see ref. [113]). (Reprinted from *Surface & Coatings Technology*, 430, B.C.E.S. Kurelo et al., Mechanical properties and corrosion resistance of α_N -rich layers produced by PIII on a super ferritic stainless steel, 126388, Copyright (2020), with permission from Elsevier).

N-content far beyond the solubility limit was detected in the expanded ferrite layer: a N content of ~12 at.% was present in UNS S44400 super-ferritic stainless steel which was PIII-nitrided at 400 °C for 3 h [113], while a value as high as ~24 at.% was detected in an AISI 430F ferritic stainless steel which subjected to ion implantation at 380 °C for 1 h with a voltage of 10 kV [60]. X-ray diffraction analysis suggested that the expansion of the ferrite b.c.c. lattice was not isotropic, with a higher value for the (200) plane than that for the (110) one [60,104,113] (Figure 6). Variations up to 6.62% for the lattice parameter calculated from the (200) peak and 5.24% for the lattice parameter calculated from the (110) peak were observed [104]. It was hypothesized that this anisotropic expansion was due to the anisotropy of the elastic modulus, with lower elastic modulus for the $\langle 200 \rangle$ direction in comparison with that of the $\langle 110 \rangle$ one [104].

Michal et al. [61] observed, on E-BRITE stainless steel subjected to carburizing treatment at 470 °C, the formation of C-rich expanded ferrite layer with a maximum C content of ~10 at.%, which caused a lattice expansion of ~0.3%.

4.1.3. Hardness of the Modified Surface Layers

The formation of the expanded ferrite allows for increased surface hardness, due to solid solution strengthening effect. The precipitation of nitrides and carbides increased the microhardness further on, and higher values were observed as the volumetric fraction of nitrides and carbides increased, or when a continuous nitride layer was able to form. For N-rich expanded ferrite layer, microhardness values up to ~1090 kg_f mm⁻² were registered [113]. Microhardness values higher than 1000 kg_f mm⁻² were observed on carburized samples [61]. The formation of Fe-based nitrides increased surface microhardness, and values up to ~1200 kg_f mm⁻² were

registered [104]. A further increase, with values as high as $1550 \text{ kg}_f \text{ mm}^{-2}$, was observed when a large volume fraction of Fe- and Cr-based nitrides formed [114].

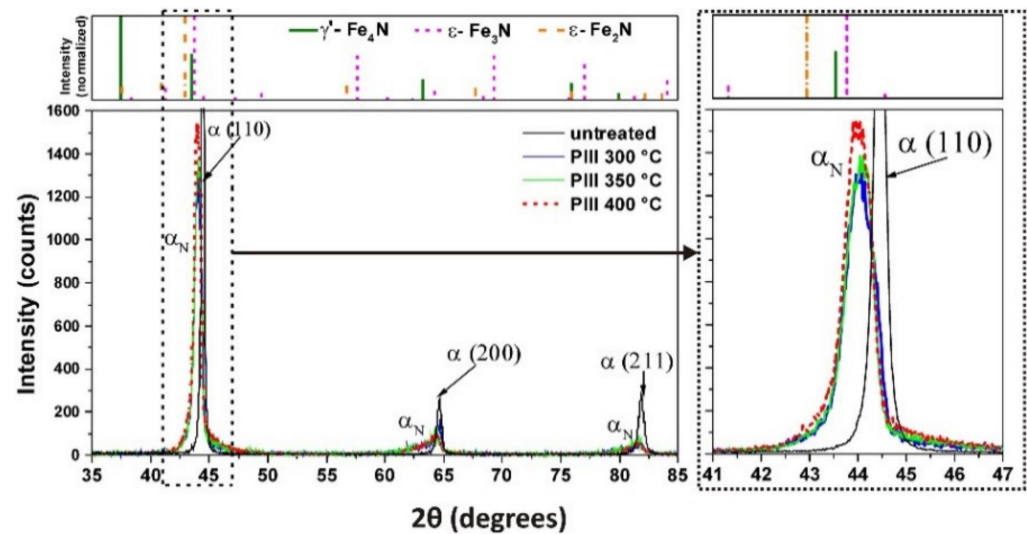


Figure 6. X-ray diffraction patterns of UNS S44400 super-ferritic stainless steel samples untreated and PIII nitrided as indicated (α : ferrite, α_N : expanded ferrite). (For further details, see ref. [113]). (Reprinted from *Surface & Coatings Technology*, 430, B.C.E.S. Kurelo et al., Mechanical properties and corrosion resistance of α_N -rich layers produced by PIII on a super ferritic stainless steel, 126388, Copyright (2020), with permission from Elsevier).

When expanded ferrite was able to form without nitrides or carbides or with a negligible amount of Fe-based compounds, fairly smooth hardness profiles were observed [61,113]. When fairly high amounts of nitrides or carbonitrides form, the microhardness profile shows the presence of high hardness values at the surface, forming a more or less extended plateau, and then a steeper decrease to matrix values [115,124].

4.1.4. Tribological Properties of the Modified Surface Layers

Owing to the increase of surface hardness, the presence of an interstitial-rich expanded ferrite layer should improve the wear resistance of ferritic stainless steels. However, in international literature, the main studies reported the wear behavior of ferritic stainless steels subjected to treatments that produced more or less large amounts of nitrides, which do not allow for an evaluation of the effect of the expanded phase only. Improvement of wear resistance was observed for samples in which Fe-based nitrides were formed, tested in ball-on-disk configuration with an alumina ball as a counterpart [90], and for specimens having both Fe- and Cr-based nitrides, subjected to micro-abrasive wear tests [123] and sliding wear tests using an Amsler machine [124].

4.1.5. Corrosion Resistance of the Modified Surface Layers

The formation of a continuous N-rich expanded ferrite layer allowed for an increase in the corrosion resistance in NaCl solutions. Polarization curves usually showed an increase in corrosion potential and pitting potential, and a decrease in anodic current density in the passive branch [113,114,120]. The precipitation of Fe-based nitrides, which are nobler than the expanded phase, can cause a microgalvanic effect, thus a worsening of the corrosion resistance may occur [113,114,123]. Kurelo et al. [113] observed an increase of the passive current density values for UNS S44400 super-ferritic stainless steel PIII nitrided at $400 \text{ }^\circ\text{C}$, in comparison to those of samples nitrided at $300 \text{ }^\circ\text{C}$, and assumed that this fact was due to the precipitation of Fe-based ϵ -nitride, and possibly of Cr nitrides. Similar nitrided samples, having a higher nitride content, were tested by Luiz et al. [104] in a 3.5% NaCl solution for up to 30 days of immersion. For both nitrided and untreated samples, an increase of the open circuit potential values for up to 15 days was observed, followed by a slight decrease.

However, the potential values of nitrided samples were nobler than those of the untreated alloy, suggesting an improvement of passive film stability after nitriding.

A continuous layer of ϵ -nitride may increase the corrosion resistance in Cl^- -containing solutions further on [126]. Increasing the treatment temperature and/or the treatment duration may promote the precipitation of Cr nitrides, which causes a marked worsening of the corrosion resistance. When AISI 430 was nitrided at 420 °C, the pitting potential increased with respect to that of the untreated steel in a 0.5 M NaCl solution, but when the treatment was prolonged up to 20 h, a marked decrease in corrosion and pitting potentials was observed [120]. When a large volume fraction of Cr nitrides was able to form, a marked decrease in corrosion resistance was reported [114,123,127].

Different corrosion behaviors were observed when low-temperature treated ferritic stainless steels were tested in Cl^- -free solutions. Spies [120] reported a significant increase of corrosion potential and decrease in the corrosion rate for AISI 430 steel samples nitrided at 300 °C for 60 h or at 350 °C for 26 h and tested in a 0.05 M H_2SO_4 solution, in comparison with the untreated alloy. A similar behavior was observed for AISI 430 samples nitrided at 250 °C for 39 h or 420 °C for 36 h [127]. On the contrary, Gontijo et al. [128] reported only a slight increase in corrosion potential and a marked increase in anodic current density for AISI 409 samples nitrided in the range of 350–500 °C and tested in a 0.1 M H_2SO_4 solution, in comparison with the untreated steel.

Regarding carburizing treatment, for the C-rich expanded ferrite an improved resistance to localized corrosion can be inferred on the basis of the high resistance to chemical etching of the modified layer [61].

4.2. Duplex Stainless Steels

Table 3 summarizes the main characteristics of the modified surface layers, in which expanded ferrite forms, obtained by the nitriding or carburizing of duplex stainless steels.

Table 3. Main characteristics of the modified surface layers containing expanded ferrite, obtained by the nitriding or carburizing of duplex stainless steels.

Properties	Nitriding	Carburizing
Formation temperature (without formation of Cr compounds) (°C)	<430	<480
Max. interstitial content in expanded ferrite (at. %)	25	18
Max. surface hardness ($\text{kg}_f \text{mm}^{-2}$)	1510	1500
Hardness profile	abrupt change	abrupt change
Dry sliding wear resistance	good	-
Localized corrosion resistance	very good	good

4.2.1. Formation of Expanded Ferrite

The basic microstructure of duplex stainless steels consists of austenite grains in a ferritic matrix. The ferrite and austenite regions have different compositions, due to the partitioning of alloy elements during cooling. When a fairly slow cooling is performed, ferrite is richer in ferrite-stabilizing elements, such as Cr and Mo, while austenite is rich in austenite-stabilizing elements, such as Ni and Mn. When a low-temperature treatment is performed on a duplex stainless steel, the interstitial atoms have a different diffusion rate in austenite and ferrite. In fact, N and C atoms diffuse faster in the b.c.c. ferrite grains than in f.c.c. austenite ones, therefore different thickness values of the modified layers were observed in the two phases [116]. Moreover, depending on treatment conditions and alloy composition, ferrite may solubilize a “colossal” amount of interstitial atoms, thus expanded ferrite is observed [129–133], or transforms into expanded austenite [116,132–136]. The original ferrite grains have a greater tendency to form nitride precipitates, due to the presence of a fairly larger amount of nitride-forming elements, such as Cr and Mo. Bielawski and Baranowska [129] observed the formation of some strongly etched regions in a part of

the modified layer formed on ferritic substrate of a X2CrNiMo 22–5–3 duplex stainless steel which was gas nitrided at 430 °C with high N potential, while the modified layer formed on austenite was unetched. This effect became more marked by increasing the treatment temperature up to 475 °C. Cr nitride was observed in UNS S31803 steel samples subjected to active screen plasma nitriding at 435 °C for 10 h [131]. The Cr-based carbide, $M_{23}C_6$, was observed in F51 steel samples which were carburized at 480 °C for 12 h [137]. Thus, the formation of Cr nitride/carbide precipitates can be avoided using treatment temperatures lower than those usually used for the treatment of austenitic stainless steels. However, by decreasing the treatment temperature further on, the formation of Fe-based nitrides may occur. In fact, ϵ -nitride precipitates were reported to form in the expanded ferrite regions of a UNS S31803 steel, plasma nitrided with the active screen process at 400 °C for 20 h [132]. Fe-based nitride precipitates were detected by X-ray diffraction analysis, and they were hypothesized to form in the expanded ferrite grains of UNS S32750 super-duplex stainless steel samples, subjected to balanced plasma nitriding at temperatures as low as 292–355 °C, due to their brittleness under indentation [133].

4.2.2. Characteristics of the Modified Surface Layers

When both expanded ferrite and expanded austenite are able to form, the surface morphology of low-temperature treated duplex stainless steels has features similar to those observed for austenitic stainless steels, with delineated grain boundaries, reliefs, and shear lines present in austenite grains, while the ferritic part remains fairly smooth [125].

Differences in the austenite and ferrite grains are also present when the cross-section microstructure is examined (Figure 7). As recounted previously, when duplex stainless steels are treated at low temperatures, the part of the modified surface layer containing ferrite is usually thicker than that containing austenite [125,130,132,138]. In the austenitic part, the layer, delineated by chemical etching, has a characteristic arc-like shape, and it is thicker close to the ferrite boundary and thinner in the central part of the austenite grain [125,130] (Figure 7a,b). This fact can be ascribed to grain boundary diffusion and lateral flow of N atoms from ferrite to austenite [139]. Apart from the differences in thickness, the whole modified surface layer was fairly smooth, and both the expanded ferrite and expanded austenite grain types were not significantly etched by chemical etching [125]. Deformation bands were present in the expanded ferrite regions (Figure 7d), due to intense compressive stresses developed during nitriding, as well as slip lines in the expanded austenite regions (Figure 7c), when the cross-section of a F51 steel, nitrided at 400 °C for 20 h and etched with oxalic acid (10%), was analyzed [130]. A similar microstructure with deformation bands was observed in UNS S31803 steel samples subjected to active screen plasma nitriding at 400 °C for 20 h [132]. Moreover, TEM analysis highlighted the presence of needle-like coherent ϵ -nitride precipitates having an orientation relationship of $[111]_{\alpha_N} // [120]_{\epsilon-Fe_3N}$.

Recently, Dalton et al. [140] performed a high-resolution spatially-resolved compositional and structural analysis of the δ -ferrite grains of 2205 duplex stainless steel samples nitrided in the range of 325–400 °C, and observed two competitive responses to nitriding. Some regions had a N content up to ~25 at.% and maintained a b.c.c. lattice without evident distortions. In these expanded ferrite grains, a spinodal decomposition occurred, with Fe-rich nanocrystals and nanometer Cr-rich domains having an apparently amorphous structure, and a preferential N segregation to the Cr-rich regions was observed. In other regions of the modified layer, austenite formed with a diffusionless transformation from ferrite, maintaining the composition of the expanded ferrite. The plates of this austenite contained a significant concentration of faults and/or twins, and tended to grow with a preferred orientation relationship from the parent ferrite, suggesting that their growth was due to a shear mechanism characteristic of martensitic reactions.

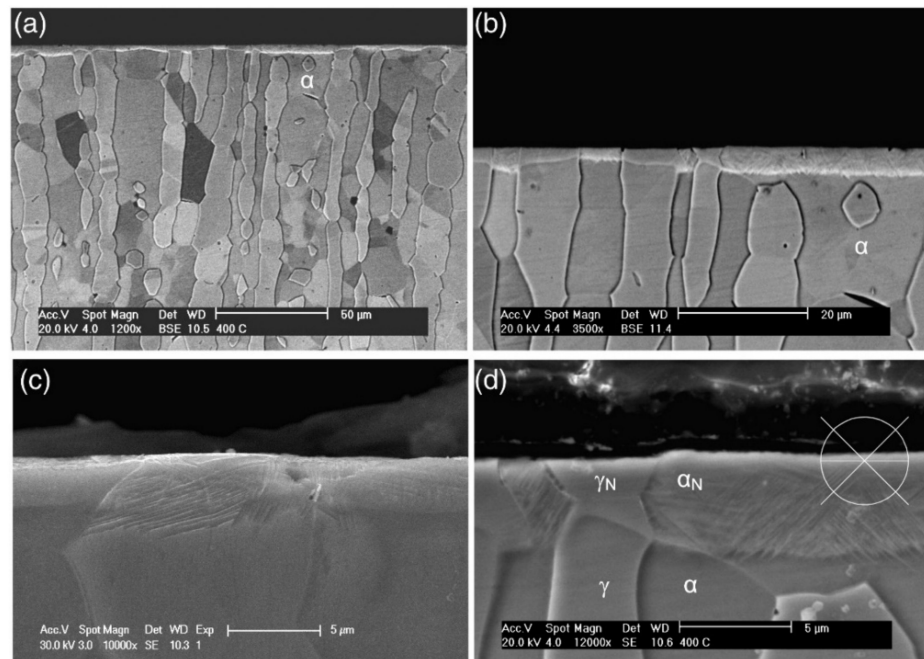


Figure 7. Micrographs of the cross-section of an AISI F51 duplex stainless steel sample plasma nitrided at 400 °C for 20 h: different thicknesses in ferrite and austenite grains (a,b), slip lines in austenite grains (c), deformation bands in ferrite grains (d) (etchant: oxalic acid (10%)) (α_N : expanded ferrite, γ_N : expanded austenite). (For further details, see ref. [130]). (Reprinted from *Surface & Coatings Technology*, 232, C.E. Pinedo et al., Low-temperature plasma nitriding of AISI F51 duplex stainless steel, 839–843, Copyright (2013), with permission from Elsevier).

A study [141] on the characteristics of the δ -ferrite present in the modified surface layers produced in 2205 duplex stainless steel and 17–7 semi-austenitic PH stainless steel subjected to carburizing at 380 °C for 150 h showed the presence of a high density of dislocations in the C-rich ferrite grains. A spinodal-like decomposition produced Fe-rich and Cr-rich regions, and the Cr-rich regions were enriched in C. Even if the C content in these modified grains was very high, with an average value as high as 18 at.%, no tetragonality was observed in the ferrite b.c.c. lattice, and carbides were not detected. It was hypothesized that C atoms were segregated to the dislocation cores, thus carbide precipitation was prevented. It was also suggested that the high dislocation density was due to the fairly large stresses applied by the neighboring austenite grains due to their volume expansion. According to Sasidhar and Meka [142], the observed high C content was in accordance with a paraequilibrium that occurred between the carburization atmosphere and the spinodally-decomposed ferrite.

Although there is a general consensus on the fact that the interstitial content is different in the ferritic part of the modified layer as compared with that of the austenitic one, conflicting results have been reported. Bielawski and Baranowska [129] detected a higher N content in the austenite part of the modified layer than in the ferritic one for X2CrNiMo 22–5–3 duplex stainless steel samples which were gas nitrided in the range of 400–475 °C. On the contrary, Pinedo et al. [130] reported a higher N content in expanded ferrite grains than in expanded austenite ones of a F51 steel which was plasma nitrided at 400 °C for 20 h. A similar result was found by Chiu et al. [131] in UNS S31803 steel samples subjected to active screen plasma nitriding for 10 h, and by Alphonsa et al. [138] in 2205 duplex grade samples nitrided at 400 °C for 4 h. When nitrocarburizing of 2205 duplex stainless steel was performed at 400 °C for 4 h, a higher N and C content was detected in austenite grains than in ferrite grains, while the thickness of the modified layer in the two grain types was comparable [138]. De Oliveira et al. [133] observed a larger N content and higher thickness in expanded austenite grains than in expanded ferrite ones for balanced plasma-nitrided

UNS S32750 super-duplex stainless steel samples. These authors ascribed this behavior to the higher Cr content of the super-duplex steel (~26 wt.%) in comparison with duplex stainless steels (~22 wt.%), and they hypothesized that, owing to the trapping mechanism in Cr sites, the ferrite may present a slower N diffusion in super-duplex stainless steels than in duplex stainless steels. Accordingly, better conditions for the N-saturation may occur, together with an earlier precipitation of nitrides, and thus the formation of thinner modified layers.

Higher C content was observed in the ferritic grains of a 2205 duplex stainless steel carburized at 380 °C for 150 h, in comparison with austenitic grains [141].

4.2.3. Hardness and Tribological Properties of the Modified Surface Layers

Low-temperature treatments improve the surface hardness of duplex stainless steels. However, alloy composition and treatment conditions influence both the interstitial atom content in the ferrite and austenite grains, present in the modified layers, and the eventual transformation of ferrite into expanded austenite and precipitation of nitrides and carbides, therefore, different hardness values in the different grain types were detected. Thus, it is not surprising that, for the same steel (2205), ferrite grains were observed to have higher hardness than austenite grains [138], or lower hardness [143]. In X2CrNiMo 22–5–3 duplex steel, the layer formed on ferrite was slightly (about 100–150 kg_f mm⁻²) harder than that formed on austenite [129]. Values up to ~1510 kg_f mm⁻² were registered in nitrided samples [132], and of ~1500 kg_f mm⁻² in carburized specimens [144]. Moreover, the formation of nitrides or carbides precipitates increased the hardness further on, and values as high as 1800 kg_f mm⁻² were measured [129,137]. The microhardness profiles of both austenite and ferrite grains showed high values at the surface and then a fairly steep decrease to matrix values [130,144].

Tribological properties were improved by the presence of expanded ferrite and/or expanded austenite. Higher scratch resistance and a lower friction coefficient were observed for nitrided SAF 2507 and SAF 2205 duplex stainless steels in comparison with the untreated alloys [143]. A lower mass loss was registered for UNS S31803 steel which was subjected to active screen plasma nitriding in the range 420–450 °C and tested in unlubricated ring-on-disk ITO type wear tests, as compared to the untreated steel [131].

4.2.4. Corrosion Resistance Properties of the Modified Surface Layers

Although low-temperature treated duplex stainless steels have modified surface layers that may contain both expanded ferrite and expanded austenite, consisting of different interstitials and alloy elements content, this bi-phase structure does not impair corrosion resistance in Cl⁻-containing solutions.

Increase of corrosion potential and decrease of anodic current density in the passive branch were observed for UNS S31803 steel samples subjected to active screen plasma nitriding at 420 °C for 10 h, and tested in 3.5% NaCl solution [131]. By using longer treatment times, the anodic current density values slightly increased, due to the precipitation of a small volume fraction of nitrides. Higher corrosion resistance in a 3.5% NaCl solution was observed for a 2205 duplex stainless steel nitrided and nitrocarburized at 350 and 400 °C for 4 h [138], but it is not clear whether this improvement was due to the presence of both expanded ferrite and austenite or to the transformation of ferrite into expanded austenite. Corrosion resistance comparable to that of the untreated alloy was observed for 2205 stainless steel specimens, carburized at 350 and 380 °C for 150 h, and tested in a 0.6 M NaCl solution [144]. An increase of corrosion resistance in NaCl solutions was observed when the modified layers consisted mainly of expanded austenite [104,136,143].

5. Expanded Austenite–S-Phase

As mentioned previously, the austenite-based expanded phase was the first supersaturated solid solution of interstitial atoms in a Fe-based lattice recognized to form as a consequence of low-temperature treatments of stainless steels. Today, the most used names

of this metastable phase are “expanded austenite”, “S-phase”, γ_N (for the N-rich form), and γ_C (for the C-rich form). In particular, “expanded austenite” and “S-phase” are mainly related to two features of this phase: the solubilization of interstitial atoms far beyond the solubility limit, thus a “colossal” supersaturation occurs [54,58], and an expansion of austenite lattice is observed [145], and the peculiar X-ray diffraction pattern of this phase, with the peaks markedly shifted towards lower angles with respect to those of austenite. Ichii et al. [17], indicated these peaks, that were not indexed in the ASTM index, as S1-S5 and the new “phase” as “S-phase”, and they assumed, also taking into account its high resistance to chemical etching and its ferromagnetism, that it was a M_4N -type nitride.

As a matter of fact, it is now recognized that expanded austenite–S-phase is not a “new” equilibrium phase, and that it derives from austenite. However, many studies have highlighted that the characteristics of this phase are beyond a simple expansion, or a “colossal” supersaturation, of the austenite lattice, even if some of them can be related to it.

Expanded austenite was observed to form not only in austenitic stainless steels, both in massive specimens [8,11,46,47,146] and coatings obtained with various techniques [147–154], but also in stainless steels, in which the high N solubilization might induce the transformation of ferrite or martensite into austenite, as duplex [104,116,132,134–136], martensitic [65,91,95], ferritic [121,122], and precipitation hardening [65,71,155,156] stainless steels.

Hereafter, the main characteristics and properties of the modified surface layers containing expanded austenite are summarized. The main characteristics of the modified surface layers obtained with nitriding or carburizing of austenitic stainless steels are reported in Table 4. Further information can be found in the reviews on this topic [11,12,46,47].

Table 4. Main characteristics of the modified surface layers containing expanded austenite, obtained by the nitriding or carburizing of austenitic stainless steels.

Properties	Nitriding	Carburizing
Formation temperature (without formation of Cr compounds) (°C)	300–450	300–550
Max. interstitial content in expanded austenite (at. %)	38	19
Max. surface hardness ($\text{kg}_f \text{mm}^{-2}$)	1450	1000
Hardness profile	abrupt change	gradual change
Load bearing capacity	low	high
Dry sliding wear resistance	very good	good
Localized corrosion resistance	very good	good

5.1. Formation of Expanded Austenite

When low-temperature treatments are carried out on austenitic stainless steels, a supersaturated solid solution of interstitial atoms in the austenite lattice is easily formed, and Fe-based nitrides are not usually observed, contrary to what occurs in martensitic and ferritic stainless steels. As for the low-temperature treatments, treatment temperature is the main parameter to be controlled in order to hinder Cr diffusion and prevent the formation of large amounts of Cr nitrides and carbides. Nitriding is usually performed at temperatures ≤ 450 °C [8,38], while carburizing is carried out at temperatures ≤ 550 °C [38]. Treatment duration is also highly important, and the transition from the solubilization of interstitial atoms to the formation of nitrides and carbides in the austenite matrix was depicted in time–temperature–transformation diagrams, evidencing that for a specific treatment temperature exists a critical time beyond which the formation of Cr nitrides or carbides occurs [38,42]. The feeding of interstitial atoms is a further important factor for obtaining expanded austenite, as observed in plasma nitriding treatments. By decreasing the treatment pressure, an enhancement of nitriding efficiency occurs, and a greater N atoms inlet is produced [103,157,158]. As a consequence, nitride precipitates are able to form at temperatures at which their formation should typically be delayed [103].

The formation of nitrides and carbides is also influenced by the alloy elements of the stainless steels. Cr is not only able to form nitrides or carbides, but it also promotes the formation of expanded austenite. Ni, which is the main austenite-stabilizing element of CrNi-based AISI 300 series austenitic stainless steels, is not a nitride-/carbide-forming element, therefore it tends to promote the formation of a nitride-free expanded austenite structure up to 450 °C. When Ni is substituted, in whole or in part, by Mn, as in the CrMn-based AISI 200 series or Ni-free austenitic stainless steels, an additional nitride-forming element is introduced in the austenite lattice. As a consequence, the diffusion of substitutional atoms should be decreased further, and lower treatment temperatures and shorter treatment durations should be employed, in comparison with those used for AISI 300 series stainless steels [91,159–161]. As an example, plasma nitriding at 400 °C, 500 Pa for 3 and 5 h, using a 80 vol.% N₂ + 20 vol.% H₂ gas mixture, allowed for the production of modified surface layers consisting mainly of expanded austenite on AISI 316L, while on AISI 202, sensible amounts of nitrides were detected [91], as well as on a Ni-free stainless steel [161]. Similarly, a modified layer mainly consisting of expanded austenite was produced on the high-Ni RA330[®] (Fe-19Cr-35Ni-1.2Si), triode plasma nitrided at 450 °C for 20 h, while by using the same treatment conditions, large volume fractions of nitride precipitates were observed on both high-Mn Stalloy[®] AG17 (Fe-17Cr-20Mn-0.5N) and AISI 304 [162].

When low-temperature treatments are performed on austenitic stainless steels, N and C diffusion in f.c.c. austenite results enhanced. Williamson et al. [57] reported that, when N-rich expanded austenite layers formed, N diffusion was four to five orders of magnitude faster than that expected for N in f.c.c. austenite and the activation energy was significantly reduced. Regarding C-rich expanded austenite, Ernst et al. [163] observed that C diffusion coefficient was more than two orders of magnitude larger for high C levels, in comparison to that of a dilute solution. The concentration profile of interstitial atoms in low-temperature treated austenitic stainless steels cannot be described by the complementary error function, which is characteristic of concentration independent diffusion. In nitrided samples, N concentration vs. depth profile has high values at the surface, a steep decrease to lower values followed by a nearly constant plateau, then a steep decrease to matrix values [11,45,46,149,159]. In carburized samples, a steep decrease from the high values at the surface, followed by a smoother decrease to matrix values, is present [11,45,46,149,159,163]. When nitrocarburizing is carried out [45,46,147,149,159], or sequential treatments are performed, i.e., nitriding followed by carburizing [164] or carburizing followed by nitriding [134,147,149,164], an outer N-rich expanded austenite layer and an inner C-rich expanded austenite layer are produced, which together allow a smoother profile to be formed, in comparison with that of nitrided steels [11,45,147,149,159,164].

Many effects may contribute to the enhanced diffusion and “colossal” supersaturation of the expanded austenite. Diffusion of interstitial atoms seems to depend on their concentration, and not on a composition gradient, with higher values for fairly high N and C content and lower values for low concentration [163,165]. Cr atoms are hypothesized to have a “trapping effect” on N atoms in the octahedral sites nearby, causing short-range ordering, while additional N atoms can be “detrapped” and diffuse rapidly through the expanded austenite layer [166–168]. A further phenomenon, which may influence the diffusion of interstitial atoms, is the high compressive residual stresses which are produced in the modified layer as a consequence of the expansion of austenite lattice, and may become an additional component of the driving force for the interstitial atoms transport [169–171].

As a metastable phase, expanded austenite tends to decompose when the service temperature is too high. The incubation time for the transformation of N-rich expanded austenite into CrN and α -Fe ranges from minutes at 500 °C to thousands of hours at 300 °C [172], while for C-rich expanded austenite decomposition and formation of carbides occur in thousands of hours at 350 °C [173].

5.2. Characteristics of the Modified Surface Layers

Figure 8 depicts the surface morphology and the cross-section microstructure of an AISI 202 sample which was plasma-nitrided at 380 °C, 340 Pa, for 3 h, together with its X-ray diffraction pattern, also showing the austenite substrate.

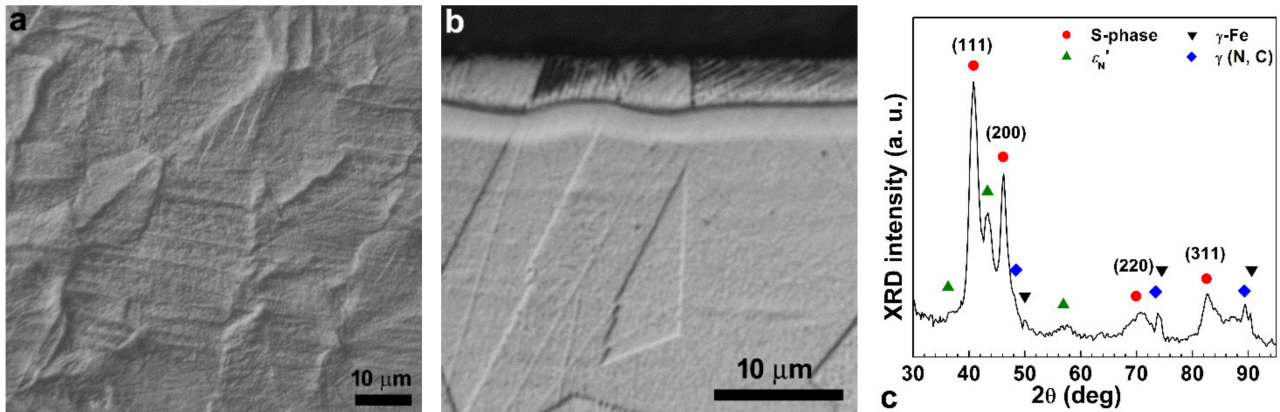


Figure 8. Surface morphology (a), cross-section micrograph (b) (etchant: acetic glyceragia) and X-ray diffraction pattern (c) of an AISI 202 austenitic stainless steel sample plasma nitrided at 380 °C, 340 Pa, for 5 h. (For further experimental details, see ref. [174]).

A characteristic feature of the surface morphology of low-temperature treated austenitic stainless steels is the etched appearance, with distinctly delineated grain boundaries, slip bands inside the grains and a swelling of the grains [11], as shown in Figure 8a. Even if plasma processes may enhance these features [174–176], they are also observed on gas nitrided samples [177], and they are caused by the local plastic deformations due to the expansion of the austenite lattice when interstitial atoms are solubilized (11 and references therein).

When the cross-section microstructure is examined, a featureless “white” layer, separated by the etched matrix, can be observed when an etchant as Marble’s reagent is used [15]. The difficulty of etching expanded austenite supported the hypothesis of the formation an unknown nitride [15]. The use of etchants as glyceragia provides evidence that the nitrided layers are instead a modification of the austenite matrix, and that the grain boundaries of the expanded austenite are the continuation of the austenite matrix grain boundaries [11,178]. When nitriding is performed, a two-layer microstructure is delineated, with an outer thicker layer, consisting mainly of expanded austenite, and an inner layer without evident features (Figure 8b). The interfaces between these layers and between the inner layer and the matrix are fairly sharp. Also taking into account the suggestions of Christiansen et al. [169], it may be hypothesized that these interfaces are due to the sudden change of the N concentration (and as a response to the chemical etching as well), and they are not thermodynamic or crystallographic interfaces. The modified layers are fairly homogenous, even if grain-to-grain variations in thickness may be observed due to the different N diffusion in differently oriented grains [179]. Moreover, rotation of the grains with respect to the substrate is observable [180].

In the outer modified layer many lines may be observable, as shown in Figure 8b, and their number and extension in the substrate depend on nitriding conditions and alloy composition [174,181]. Tapered sections allow to appreciate the complex structure of these slip lines, due to localized plastic deformation phenomena occurring in the outer part of the modified layer [161,181]. A consequence of the plastic deformations is the formation of the so-called N-induced h.c.p. martensite, ϵ'_N , which is a solid solution of nitrogen in the h.c.p. ϵ' martensite [182]. In fact, when plastic deformations occur in austenitic stainless steels, the fairly low stacking fault energy of these alloys, lowered further by N solubilization [183], may allow the formation of wide stacking faults, with the characteristic ABAB stacking of a h.c.p. structure [184]. According to Tao et al. [185], ϵ'_N forms from expanded austenite, and not from an unexpanded ϵ' , through a martensitic shear transformation above a critical

N concentration. Tong et al. [186] objected that these h.c.p. regions should be regarded as “clustered” stacking faults, instead of plates of N-rich h.c.p. ϵ' martensite. The presence of ϵ_N' was observed by means of X-ray diffraction analysis [174,181,185], as depicted in Figure 8c, and in SAED patterns [182]. TEM analysis showed that the h.c.p. structure is coherent with the matrix, and it has the Shoji–Nishiyama orientation relationship typical of austenite to h.c.p. martensite transformation [176,182,185]. The formation of N-induced martensite, ϵ_N' , is dependent on both solubilized N content and steel composition, and it is favored when the stacking fault energy of the steel is low, such as for the high-Mn austenitic stainless steels [174,176,181]. The formation of h.c.p. ϵ -Fe₂₋₃N nitride from ϵ_N' , due to an ordering of N atoms and a distortion of ϵ_N' lattice, may also occur [187].

The inner modified layer consists of a solid solution of interstitial atoms (N, C) in slightly expanded austenite, γ (N, C) [11,174,181]. It has been hypothesized that this layer is related to a local increase of C atoms, which were pushed by diffusing N atoms [188], or to the N concentration profile [134], or to the high residual stress, induced between the expanded austenite layer and the substrate [189].

A similar two-layer microstructure is obtained with treatments which use N- and C-containing gas mixtures in a single step (nitrocarburizing) [45,190], or sequentially [191]. The outer modified layer consists of N-rich expanded austenite, while in the inner layer C-rich expanded austenite is present. Low-temperature carburizing produces a single modified layer [45,134,192,193].

As the treatment temperature, duration, or the interstitial atoms feeding increase, Cr compounds precipitates tend to form, especially at grain boundaries [103].

The maximum observed N content in expanded austenite is ~38 at.% [58], while the maximum C content is ~19 at.% [59].

5.3. Expanded Austenite: Is It Really a Solid Solution?

The nature of the modified surface layer formed by low-temperature treatments in austenitic stainless steels has been debated from the beginning, thanks to the high corrosion resistance of the layer to chemical etching. When it became clear that the modified layer was a modification of the austenite matrix, the hypothesis that expanded austenite was a supersaturated solid solution of interstitial atoms in the f.c.c. austenite lattice was the natural consequence.

Most of the studies on expanded austenite are biased by the fact that this phase forms on the top of massive specimens. The high content of solubilized interstitial atoms, in particular N atoms, causes a huge expansion of the lattice, which cannot be accommodated only elastically, but causes local plastic deformations [11]; moreover, high compressive stresses develop [42]. TEM analysis showed the presence of dislocations, twins, stacking faults, slip bands, and a lamellar structure, ascribable to N-induced h.c.p. martensite, ϵ_N' [176,182,186]. Mössbauer spectroscopy observations suggested the presence, together with expanded austenite, of b.c.c. α' martensite with low N content [194]. The SAED patterns of expanded austenite have broad diffuse electron spots, therefore an almost isotropically expanded f.c.c. structure might be hypothesized [46,186]. Additional weak reflections, corresponding to forbidden reflections of a f.c.c. structure, were observed by some authors [186,195,196], thus it was hypothesized the formation of a simple cubic structure, in which N atoms occupy only one of the four interstitial octahedral sites, analogous to the γ' -Fe₄N structure. This phase was observed in the whole explored area in a domain structure [196] or in very small regions, suggesting a short-range ordering process [195]. When X-ray diffraction analysis of massive specimens was taken into account, neither isotropic expansion nor the presence of γ' -Fe₄N were observed. The X-ray diffraction pattern of expanded austenite in massive specimens has a peculiar feature, with peaks shifted towards lower angles as compared to those of austenite, in accordance with an expansion of the parent lattice, but with an apparently anisotropic expansion [45,103,197,198]. In fact, assuming a f.c.c. lattice as an indexing base, the lattice parameter value calculated from the d -spacing of the (200) plane is always greater than that calculated from the d -spacing of the (111), (220),

(311) or (222) planes [45,103,197,198]. This feature was observed both in N- and C-rich expanded austenite, even if the difference is greater for the N-rich expanded phase than for the C-rich one [197]. Different lattice structures (mixed f.c.c. lattice, tetragonal, monoclinic, rhombohedral, and equal-sided triclinic lattice) were tested without obtaining satisfying results [198]. Taking into account microstructure observations, it may be hypothesized that lattice expansion, residual stresses, and stacking faults, which all have an effect on the peak shifts, contribute to the anomalous shift of expanded austenite peaks (11 and references therein, 198).

Other observations add interesting details to the picture. X-ray photoelectron spectroscopy (XPS) analysis results suggest that a preferential bonding of N to Cr atoms establishes, but the binding energy of N is higher than that in Cr nitride [199,200]. Analyzing the N-rich expanded austenite present at the surface of AISI 304L samples, plasma nitrided at 400 °C for 3 h, Martinavičius et al. [201] observed, by means of conversion electron Mössbauer spectroscopy (CEMS) and X-ray absorption near edge structure spectroscopy (XANES) techniques, that for Cr there is a tendency toward a CrN-like environment with a Cr-N bonding, while the Fe environment in expanded austenite is very similar to that of γ' -Fe₄N, but with a larger disorder. Thus, it was hypothesized that the expanded austenite phase is composed by nanometric CrN-like precipitates, coherent with the matrix, incorporated in a γ' -Fe₄N matrix. Atom probe tomography (APT) observations seem to support this hypothesis [202]. On the basis of these studies it was suggested that the “colossal supersaturation” implies a spinodal decomposition, which produces the nano-sized precipitates [203]. In Fe–Cr–Ni alloys with a Cr content higher than 12 wt.%, nitrided at 380 °C for 3 h, the outer N-rich zone consisted of γ' -Fe₄N-like long-range order (LRO) regions and Cr-N short-range order (SRO) regions, which were indicated as γ'_N , while the inner zone was an interstitially disordered expanded austenite with SRO regions of Cr and N atoms [204]. The two zones were indistinguishable from each other and formed a single “white” modified layer. It should be noted that γ'_N was regarded as an ordered phase having a N content far beyond that of γ' -Fe₄N (19.3–20 at. % [50]), i.e., a supersaturated phase [205].

The use of thin foils for producing expanded austenite allowed for the removal of the constraints of the matrix, and thus the effects of plastic deformations. X-ray diffraction analysis of thin foil specimens, consisting of expanded austenite of uniform composition, showed that both N-rich [58] and C-rich [206] expanded austenite have a f.c.c. lattice. Extended X-ray absorption fine structure (EXAFS) spectroscopy studies confirmed the presence of a preferential bonding between Cr and N atoms, suggesting the formation of SRO structures [207]. A similar result was found for carburized samples, with C atoms having a strong affinity with Cr atoms, thus probably promoting SRO [208]. X-ray diffraction analysis and CEMS observations of AISI 316 foils, gas nitrided in order to retain a homogenous content of 35.5 at.%, suggested the formation of a LRO structure analogous to γ' -Fe₄N [209]. A study that supports the hypothesis that at high N-content expanded austenite tends to become an ordered phase has been recently reported by Che and Lei [210]. By using a plasma-based low-energy ion implantation process, these authors nitrided at 380 °C for 10 min TEM foils of two Fe–Cr–Ni steels, one Ni-rich (Cr 17.66 wt.%, Ni 27 wt.%), and the other having a Ni content comparable to that of AISI 304 and AISI 316 (Cr 17.66 wt.%, Ni 12.6 wt.%), and compared the obtained results with massive specimens. For all of the samples the N content was estimated to be fairly high, in the range 30.3–33.4 at.%, far beyond that of γ' -Fe₄N. While in massive specimen twins (Ni-rich steel) or multiple stacking faults forming h.c.p. structures (AISI 304-like steel) were observed, the TEM foils did not show evidences of plastic deformations, thus they could be considered stress-free. The SAED patterns of expanded austenite in TEM foils of both steel types showed the strong diffraction spots of a f.c.c. structure together with the weak spots of a γ' -Fe₄N-like superstructure. Since the formation of this ordered structure was independent of stress and plastic strain, it was assumed that it was a characteristic feature of expanded austenite with a fairly high N content.

It is worth noting that the tendency to form a (short) range ordered structure, similar to that of γ' -Fe₄N, is present in the solid solution of N in f.c.c. γ -Fe [52], as reported in Section 2. The presence of Cr strengthens this tendency further on, since Cr has higher affinity for N than Fe. On the basis of the literature data, it may be hypothesized that, as N content increases in expanded austenite and the octahedral interstitial sites are occupied, there is a transition from a more disordered structure with Cr-N SRO regions to a structure in which γ' -Fe₄N-like LRO domains tend to form, while the f.c.c. lattice is maintained. For thin foils of gas nitrided AISI 304 and AISI 316, a maximum N content of ~38 at.% was detected [58]. A N content up to ~45 at.% was obtained in the expanded austenite that was produced as thin films by means of magnetron sputtering of AISI 316L in a N₂-Ar gas mixture [211]. As the N₂ volume fraction in the gas mixture was increased, a N content of 50 at.% was reached in the deposited phase. This MN-type phase maintained the f.c.c. lattice and had a constant lattice parameter of about 0.433 nm. It is known that the metastable FeN nitride may have two different structures, both having the Fe atoms arranged in a f.c.c. lattice, a ZnS-type, γ'' -FeN, with each N atom coordinated by four Fe atoms at the corners of a regular tetrahedron, and a NaCl-type, γ''' -FeN, with each N atom coordinated by six Fe atoms at the corners of a regular octahedron, while CrN has a NaCl-type structure [211]. Unfortunately, experimental data on the arrangement of N atoms in this MN-type phase were not reported. Thus, it remains an open question whether, in austenitic stainless steels, N atoms are able to progressively occupy all the octahedral sites of f.c.c. lattice, thus there is a transition from a N-atoms disordered structure to a more ordered γ' -Fe₄N-like structure and then to a FeN/CrN NaCl-type structure, or whether also tetrahedral sites are occupied when a high N content is present, leading to a FeN ZnS-type structure.

5.4. Hardness of the Modified Surface Layers

The superior hardness of expanded austenite allows for a significant improvement in surface hardness of austenitic stainless steels. For N-rich expanded austenite, values up to ~1450 kg_f mm⁻² were observed [212]. Values as high as 1600 kg_f mm⁻² were reported when Cr nitride precipitates were also able to form and a small indenter load was used [38,103]. The microhardness profiles tend to reflect the average concentration profiles, as depicted in Figure 9. In nitrided samples, microhardness profiles usually show a plateau with high hardness values near the outer surface, and then a steep decrease to matrix values, related to the peculiar N-content profile [84,134,149,190,213]. C-rich expanded austenite reaches values of ~1000 kg_f mm⁻² [214], and the microhardness profile is smooth in carburized samples [84,134,149,190,213]. When treatments which use N- and C-containing gas mixtures are performed as a single step (nitrocarburizing) or in succession, the presence of both N-rich and C-rich expanded austenite allows to obtain high values at the surface with a gradual change towards matrix values [84,147,149,190,215].

5.5. Tribological Properties of the Modified Surface Layers

The hardened surface layers, obtained by means of low-temperature treatments, allow for an increase in the poor tribological properties of austenitic stainless steels. The efficiency in improving wear resistance depends on different factors: the microhardness profile, due to the treatment type, the test conditions, and the used counterface.

While untreated austenitic stainless steels usually suffer severe adhesive wear, an oxidative mild wear is observed for treated steels tested in pin-on-disk configuration, therefore wear loss significantly decreases in both dry [84,158,216] and wet [216,217] conditions. The importance of the materials constituting the tribosystem in influencing wear resistance was put in light for nitrided [216] and carburized [218] samples. For example, when AISI 316 samples, nitrided at 450 °C for 5 h, were tested in dry sliding conditions using a bearing steel as counterpart, the wear volume was approximately two orders of magnitude lower than that of the untreated steel, but using an alumina ball as counterpart the wear volume was only reduced by about a factor of eight [216]. The hard modified layer obtained with

nitriding treatments improves efficiently abrasive resistance [213], and it allows for a low wear rate as long as the modified layer is not broken [197,215,219]. Carburized samples have a lower resistance to abrasion, as compared to nitrided samples [213], due to their lower hardness, but they show a higher load-bearing capacity [197,215], owing to the lower hardness gradient. The combination of high microhardness values at the surface with a fairly smooth hardness profile, obtained with nitrocarburizing [84] or by combining nitriding and carburizing [215], allows for a better load-bearing capacity than that obtained by nitriding or carburizing, hence a significant improvement of wear resistance was observed.

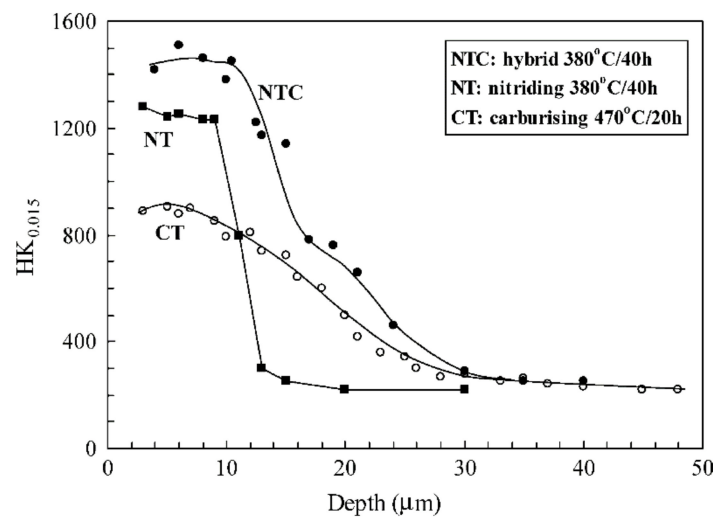


Figure 9. Microhardness profiles of AISI 321 samples plasma nitrided (380 °C, 40 h), carburized (470 °C, 20 h), and nitrocarburized (NTC hybrid process) (380 °C, 40 h). For further details, see ref. [190]. (Reprinted from *Materials Science and Engineering A*, 404, Y. Sun, Hybrid plasma surface alloying of austenitic stainless steels with nitrogen and carbon, 124–129, Copyright (2005), with permission from Elsevier).

5.6. Corrosion Properties of the Modified Surface Layers

The presence of expanded austenite as the main phase in the outer modified surface layer, without the formation of significant amounts of compound precipitates, allows for the significant improvement in corrosion resistance of austenitic stainless steels in Cl^- -containing solutions. N-rich expanded austenite showed an excellent corrosion resistance in NaCl solutions [11,40,46,104,174,181,220,221] (Figure 10). It is known that N alloying of austenitic stainless steels promotes passivity, widens the passive range, and improves the resistance to intergranular corrosion and stress corrosion cracking [8]. It may be assumed that the enhancement of corrosion resistance for N-rich expanded austenite is due to mechanisms analogous to those suggested for N-containing austenitic stainless steels, in particular the reaction of released N atoms with H^+ to form ammonium ions, NH_4^+ , that locally increase the pH where pits or crevices are forming, hence repassivation is promoted [46,220,222]. It was observed that the neutralizing effect of NH_4^+ ions is significant only above a certain range of pH [220]. In fact, Zhu and Lei [220] reported that the formation of an expanded austenite layer, produced by nitriding AISI 1Cr18Ni9Ti at 380 °C for 4 h, allowed to avoid pitting corrosion when the samples were put in contact with a 3% NaCl solution at pH in the range 4–13, while for the untreated steel active-passive transition occurred. At lower pH values, even if pitting phenomena occurred, higher pitting potential was registered for nitrided samples than for the untreated alloy.

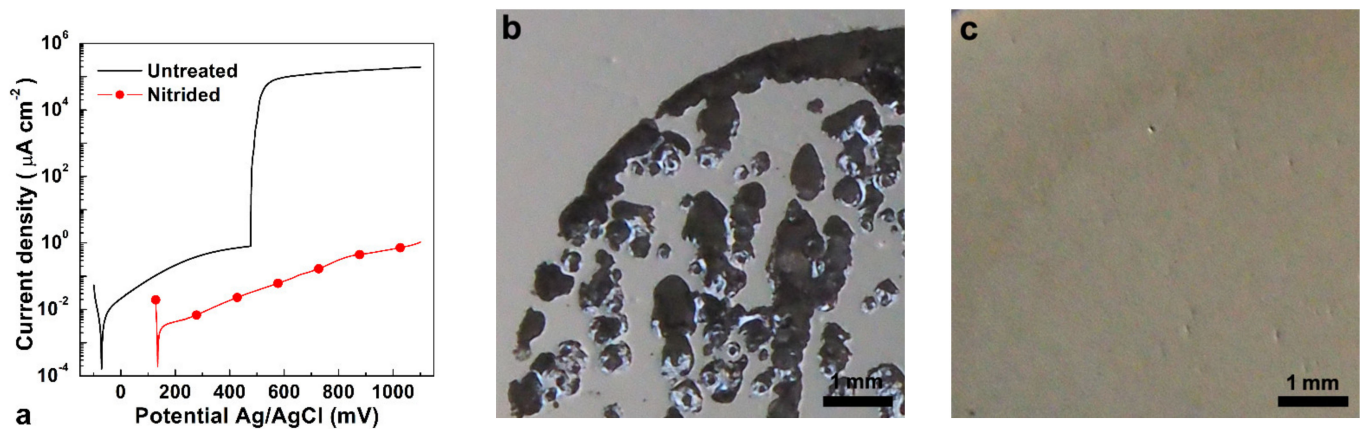


Figure 10. Corrosion behavior of AISI 202 samples untreated and plasma nitrided at 380 °C, 340 Pa, for 3 h: polarization curve (a), details of the surface morphology after corrosion test of untreated (b) and nitrided (c) samples (solution: 5% NaCl, aerated). (For further experimental details, see ref. [174]).

The protectiveness of the expanded austenite layer and its ability in hindering and delaying the occurrence of corrosion phenomena increase as the N content and the thickness of the modified layer become higher, and the precipitation of significant amounts of nitrides is avoided, therefore treatment conditions should be carefully chosen in order to obtain a N-rich, nitride-free, and thick modified layer [40,103,161,181,212,221]. The stability of the passive film was improved for up to 30 days of immersion in 3.5% NaCl for UNS S31254 super-austenitic stainless steel nitrided at 400 °C [104]. Electrochemical Impedance Spectroscopy (EIS) analysis showed that nitrided samples usually have higher impedance values than those of the untreated alloy, suggesting a better resistance to general corrosion [174,223,224]. Potentiodynamic tests demonstrated that nitrided samples can achieve a higher corrosion and pitting potential, and lower current density in the passive branch, in comparison with the untreated steel [158,174,177,221,225] (Figure 10a), thus the surface damage is reduced, as depicted in Figure 10b,c. By comparing the corrosion behavior of different austenitic stainless steels (AISI 316L, AISI 202 and Ni-free P558), nitrided at 360 and 380 °C for 3 h, it was hypothesized that the higher corrosion potential and lower anodic passive currents were influenced mainly by the N content in expanded austenite, while for pitting potential the role of alloy elements was also important [174]. Galvanostatic tests suggested that, after the occurrence of localized corrosion phenomena, repassivation may occur when the depth of pits or crevices is not too high [174]. N-rich expanded austenite layer also allows for an increase in the resistance to crevice corrosion [221].

Nitrided samples showed an enhanced corrosion resistance in Cl⁻ saline solutions, such as those used to simulate body fluids [40,226,227], and in HCl solution [225]. Moreover, nitrocarburizing [190,226] and carburizing [192,193,226] improve corrosion resistance in Cl⁻-containing solutions. For C-rich expanded austenite, it was suggested that the carburized layer decreases the mobility of charge carriers in the passive film, decreasing oxygen vacancy concentration as the C content is higher, due to the strong Cr-C bonds forming at the metal-passive-film interface [192].

The significant improvement of corrosion resistance in Cl⁻-containing solutions is reduced in NaCl + H₂SO₄ solutions [222], or in NaCl-free H₂SO₄ solutions, for which enhancement [228] and decrease [229] in corrosion resistance was observed. It was suggested that, in these conditions, the corrosion behavior is related to the presence of surface defects, as slip lines, microtwins, and dislocations, corresponding to high energy zones, which dissolve quickly and hinder repassivation [46].

6. Conclusions

Low-temperature thermochemical treatments of stainless steels allow to produce supersaturated solid solutions which are able to improve surface hardness, and hence

wear resistance, without impairing corrosion resistance. The main characteristics of these “expanded” phases are summarized in Table 5.

Table 5. Main characteristics of expanded phases (N and C refer to nitriding and carburizing, respectively).

Properties	Expanded Martensite	Expanded Ferrite ¹	Expanded Austenite
Formation temperature (°C)	200–350 (N) 200–450 (C)	<380 (N) <470 (C)	300–450 (N) 300–550 (C)
Max. interstitial content (at.%)	22 (N) 10 (C)	24 (N) 10 (C)	38 (N) 19 (C)
Max. surface hardness ² (kg _f mm ⁻²)	1120 (N) 970 (C)	1090 (N) 1000 (C)	1450 (N) 1000 (C)
Hardness profile (without nitrides/carbides)	gradual change (N,C)	gradual change (N,C)	abrupt change (N) gradual change (C)
Localized corrosion resistance (without nitrides/carbides)	good (N,C)	good (N,C)	very good (N) good (C)
Tendency to form Fe-based compounds	high	high	low

¹ Data refer to the phase formed in ferritic stainless steels. ² Values referred to the expanded phases only.

As highlighted by many studies, the characteristics and properties of the modified surface layers formed on stainless steels depend on both the treatment conditions and alloy composition. For hindering the precipitation of Cr nitrides/carbides, which cause a decrease of corrosion resistance, the treatment temperature should be sufficiently low that the diffusion of substitutional atoms has significantly slowed down. Due to the structure and alloy composition, for martensitic and ferritic stainless steels, the maximum treatment temperature is lower than that used for austenitic stainless steels. However, even if the precipitation of Cr compounds can be easily avoided, the possibility of obtaining a modified surface layer consisting of expanded martensite or expanded ferrite only may be a challenging task, since Fe-based nitrides/carbides tend to form together with these supersaturated solid solutions. Fe-based nitrides and carbides improve hardness and wear resistance in dry sliding conditions further on, but the presence of a multiphase structure at the surface influences the corrosion behavior. In austenitic stainless steels, the formation of Fe-based compounds can be usually avoided, and the expanded austenite–S-phase that forms in these steels has been recognized as a valuable mean to improve hardness, tribological properties, and corrosion resistance. It is worth noting that all of the “expanded” phases, as metastable phases, tend to transform when they are exposed to fairly high temperatures. Few data about the maximum service temperature are available for martensitic stainless steels, and they suggest that the decomposition of the modified surface layers may occur at 200 °C after few hours. On the contrary, expanded austenite seems to be more stable, and extrapolation of experimental data suggests that the modified layers consisting of this phase have a long-term stability (>10 years) when a maximum service temperature of about 200 °C is employed.

As a matter of fact, from a scientific point of view, many questions on expanded phases are still open, and they can stimulate further research activity on the low-temperature treatment of stainless steels. The thermodynamic and kinetic of formation of expanded phases, the influence of treatment conditions, as well as of alloy composition, and the structure of these phases are important topics, which need to be fully clarified for optimizing the thermochemical processes and for obtaining modified surface layers with characteristics tailored for the applications.

From a technological point of view, the numerous studies carried out on the low-temperature treatments of austenitic stainless steels have led to the scale-up of these treatments from research laboratories to production processes, and now the thermochemical treatments for obtaining modified surface layers consisting of expanded austenite are an industrial practice. The possibility of applying these treatments also to the other stainless steel types can

allow to broaden the field of stainless steel components, which can benefit from improved surface hardness and good corrosion resistance for prolonging their service life.

Funding: This research received no external funding.

Institutional Review Board Statement: Not applicable.

Informed Consent Statement: Not applicable.

Data Availability Statement: Data sharing is not applicable.

Acknowledgments: IOP Publishing and Elsevier are acknowledged for the permission to use the figures.

Conflicts of Interest: The author declares no conflict of interest.

References

1. McGuire, M.F. *Stainless Steels for Design Engineers*; ASM International: Materials Park, OH, USA, 2008; ISBN 9780871707178.
2. Washko, S.D.; Aggen, G. Wrought Stainless Steels. In *ASM Handbook*; ASM International: Materials Park, OH, USA, 1997; Volume 1, pp. 841–907.
3. Jacob, A.; Povoden-Karadeniz, E.; Kozeschnik, E. Revised thermodynamic description of the Fe-Cr system based on an improved sublattice model of the σ phase. *Calphad* **2018**, *60*, 16–28. [[CrossRef](#)]
4. Lacombe, P.; Béranger, G. Structure and Equilibrium Diagrams of Various Stainless Steel Grades. In *Stainless Steels*; Lacombe, P., Baroux, B., Béranger, G., Eds.; Les Editions de Physique: Les Ulis, France, 1993; pp. 13–58. ISBN 9782868831897.
5. Talha, M.; Behera, C.K.; Sinha, O.P. A review on nickel-free nitrogen containing austenitic stainless steels for biomedical applications. *Mater. Sci. Eng. C* **2013**, *33*, 3563–3575. [[CrossRef](#)] [[PubMed](#)]
6. Lampman, S. Introduction to Surface Hardening of Steels. In *ASM Handbook*; ASM International: Materials Park, OH, USA, 1997; Volume 4, pp. 259–267.
7. O'Brien, J.M.; Goodman, D. Plasma (ion) nitriding. In *ASM Handbook*; ASM International: Materials Park, OH, USA, 1997; Volume 4, pp. 420–424.
8. Lo, K.H.; Shek, C.H.; Lai, J.K.L. Recent developments in stainless steels. *Mater. Sci. Eng. R Rep.* **2009**, *65*, 39–104. [[CrossRef](#)]
9. Davis, J.R. Surface Engineering of Stainless Steels. In *ASM Metal Handbook*; ASM International: Materials Park, OH, USA, 1994; Volume 5, pp. 741–761. [[CrossRef](#)]
10. Cardoso, R.P.; Mafra, M.; Brunatto, S.F. Low-temperature Thermochemical Treatments of Stainless Steels—An Introduction. In *Plasma Science and Technology—Progress in Physical States and Chemical Reactions*; Miesio, T., Ed.; InTech: Rijeka, Croatia, 2016; pp. 107–130, ISBN 9789535122807. [[CrossRef](#)]
11. Borgioli, F. From Austenitic Stainless Steel to Expanded Austenite-S Phase: Formation, Characteristics and Properties of an Elusive Metastable Phase. *Metals* **2020**, *10*, 187. [[CrossRef](#)]
12. Casteletti, L.C.; Neto, A.L.; Totten, G.E. Nitriding of Stainless Steels. *Metallogr. Microstruct. Anal.* **2014**, *3*, 477–508. [[CrossRef](#)]
13. Michal, G.M.; Ernst, F.; Kahn, H.; Cao, Y.; Oba, F.; Agarwal, N.; Heuer, A.H. Carbon supersaturation due to paraequilibrium carburization: Stainless steels with greatly improved mechanical properties. *Acta Mater.* **2006**, *54*, 1597–1606. [[CrossRef](#)]
14. Zhang, Z.L.; Bell, T. Structure and corrosion resistance of plasma-nitrided AISI 316 stainless steel. In *Heat Treatment Shanghai '83, Proceedings of the Third International Congress on Heat Treatment of Materials, Shanghai, China, 7–11 November 1983*; Bell, T., Ed.; The Metals Society: London, UK, 1984; p. 6.25.
15. Zhang, Z.L.; Bell, T. Structure and Corrosion Resistance of Plasma Nitrided Stainless Steel. *Surf. Eng.* **1985**, *1*, 131–136. [[CrossRef](#)]
16. Ichii, K.; Fujimura, K.; Takase, T. Microstructure, Corrosion Resistance, and Hardness of the Surface layer in Ion Nitrided 18-8 Stainless Steel. *Netsu Shori* **1985**, *25*, 191–195.
17. Ichii, K.; Fujimura, K.; Takase, T. Structure of the ion-nitrided layer of 18-8 stainless steel. *Technol. Rep. Kansai Univ.* **1986**, *27*, 135–144.
18. De Benedetti, B.; Angelini, E.; Zucchi, F. Nitruazione ionica di acciai inossidabili. In *Proceedings of the 10th National Congress on Thermal Treatments*, Salsomaggiore, Italy, 16–18 October 1984; Associazione Italiana di Metallurgia: Milan, Italy, 1984; pp. 81–88.
19. De Benedetti, B.; Angelini, E.; Zucchi, F. Nitruazione ionica di acciai inossidabili. *Metall. Ital.* **1985**, *77*, 615–621.
20. Angelini, E.; Burdese, A.; De Benedetti, B. Ion-nitriding of austenitic stainless steels. *Metall. Sci. Technol.* **1988**, *6*, 33–39.
21. Yasumaru, N.; Kamachi, K. Nitrogen-induced Phase Transformation in Type 304 Austenitic Stainless Steel. *J. Jpn. Inst. Met.* **1986**, *50*, 362–368. [[CrossRef](#)]
22. Lerner, R.M. Glow-discharge nitriding of Nitralloy 135M and AISI304 stainless steel. *J. Iron Steel Inst.* **1972**, *210*, 631–632.
23. Spalvins, T. Tribological and microstructural characteristics of ion-nitrided steels. *Thin Solid Film.* **1983**, *108*, 157–163. [[CrossRef](#)]
24. Kolster, B.H. Verschleiß- und korrosionsfeste Schichten auf austenitischen Stählen. *VDI-Berichte* **1983**, *506*, 107–113.
25. Ozbaysal, K.; Inal, O.T. Structure and properties of ion-nitrided stainless steels. *J. Mater. Sci.* **1986**, *21*, 4318–4326. [[CrossRef](#)]
26. Dingremont, N.; Bergmann, E.; Hans, M.; Collignon, P. Comparison of the corrosion resistance of different steel grades nitrided, coated and duplex treated. *Surf. Coat. Technol.* **1995**, *76–77*, 218–224. [[CrossRef](#)]
27. Sun, Y.; Bell, T.; Wood, G. Wear behaviour of plasma-nitrided martensitic stainless steel. *Wear* **1994**, *178*, 131–138. [[CrossRef](#)]

28. Tesi, B.; Bacci, T.; Poli, G. Analysis of surface structures and of size and shape variations in ionitrided precipitation hardening stainless steel samples. *Vacuum* **1985**, *35*, 307–314. [[CrossRef](#)]
29. Marchev, K.; Cooper, C.V.; Giessen, B.C. Observation of a compound layer with very low friction coefficient in ion-nitrided martensitic 410 stainless steel. *Surf. Coat. Technol.* **1998**, *99*, 229–233. [[CrossRef](#)]
30. Alphonsa, I.; Chainani, A.; Raole, P.M.; Ganguli, B.; John, P.I. A study of martensitic stainless steel AISI 420 modified using plasma nitriding. *Surf. Coat. Technol.* **2002**, *150*, 263–268. [[CrossRef](#)]
31. Bacci, T.; Borgioli, F.; Galvanetto, E.; Pradelli, G. Glow-discharge nitriding of sintered stainless steels. *Surf. Coat. Technol.* **2001**, *139*, 251–256. [[CrossRef](#)]
32. Borgioli, F.; Galvanetto, E.; Bacci, T.; Pradelli, G. Influence of the treatment atmosphere on the characteristics of glow-discharge treated sintered stainless steels. *Surf. Coat. Technol.* **2002**, *149*, 192–197. [[CrossRef](#)]
33. Byeli, A.V.; Kukareko, V.A.; Lobodaeva, O.V.; Shykh, S.K.; Davis, J.A.; Wilbur, P.J. Structure and wear resistance of 20X13 steel ion-implanted with nitrogen at a high beam-current density. *Surf. Coat. Technol.* **1997**, *96*, 255–261. [[CrossRef](#)]
34. Kim, S.K.; Yoo, J.S.; Priest, J.M.; Fewell, M.P. Martensitic Stainless Steel Nitrided in a Low-Pressure rf Plasma. In *Stainless Steel 2000: Proceedings of an International Current Status Seminar on Thermochemical Surface Engineering of Stainless Steel*; Bell, T., Akamatsu, K., Eds.; CRC Press: New York, NY, USA, 2001; pp. 149–158. [[CrossRef](#)]
35. Corengia, P.; Ybarra, G.; Moira, C.; Cabo, A.; Broitman, E. Microstructure and corrosion behaviour of DC-pulsed plasma nitrided AISI 410 martensitic stainless steel. *Surf. Coat. Technol.* **2004**, *187*, 63–69. [[CrossRef](#)]
36. de Oliveira, A.M.; Lombardi Neto, A.; Tottem, G.E.; Casteletti, L.C. Ion nitriding and nitrocarburizing of stainless steels and its influence in the corrosion resistance. In *Proceedings of the 20th International Conference on Surface Modification Technologies*, Vienna, Austria, 25–29 September 2006; Sudarshan, T.S., Stiglich, J.J., Eds.; ASM International: Materials Park, OH, USA, 2007; pp. 118–123.
37. Somers, M.A.J.; Christiansen, T. Kinetics of microstructure evolution during gaseous thermochemical surface treatment. *J. Phase Equilibria Diffus.* **2005**, *26*, 520–528. [[CrossRef](#)]
38. Bell, T. Surface engineering of austenitic stainless steel. *Surf. Eng.* **2002**, *18*, 415–422. [[CrossRef](#)]
39. Bell, T. Current Status of Supersaturated Surface Engineered S-Phase Materials. *Key Eng. Mater.* **2008**, *373–374*, 289–295. [[CrossRef](#)]
40. Fossati, A.; Galvanetto, E.; Bacci, T.; Borgioli, F. Improvement of corrosion resistance of austenitic stainless steels by means of glow-discharge nitriding. *Corros. Rev.* **2011**, *29*, 209–221. [[CrossRef](#)]
41. Luo, Q.; Yang, S. From Micro to Nano Scales -Recent Progress in the Characterization of Nitrided Austenitic Stainless Steels. *Int. J. Nanomed. Nanosurgery* **2015**, *1*, 1. [[CrossRef](#)]
42. Somers, M.; Kücükyıldız, Ö.; Ormstrup, C.; Alimadadi, H.; Hattel, J.; Christiansen, T.; Winther, G. Residual Stress in Expanded Austenite on Stainless Steel; Origin, Measurement, and Prediction. *Mater. Perform. Charact.* **2018**, *7*, 693–716. [[CrossRef](#)]
43. Somers, M.A.J.; Christiansen, T.L. Low Temperature Surface Hardening of Stainless Steel. In *Thermochemical Surface Engineering of Steels*; Mittemeijer, E.J., Somers, M.A.J., Eds.; Woodhead Publishing: Oxford, UK, 2015; pp. 557–579, ISBN 9780857095923. [[CrossRef](#)]
44. Czerwec, T.; Renevier, N.; Michel, H. Low-temperature plasma-assisted nitriding. *Surf. Coat. Technol.* **2000**, *131*, 267–277. [[CrossRef](#)]
45. Czerwec, T.; He, H.; Marcos, G.; Thiriet, T.; Weber, S.; Michel, H. Fundamental and Innovations in Plasma Assisted Diffusion of Nitrogen and Carbon in Austenitic Stainless Steels and Related Alloys. *Plasma Process. Polym.* **2009**, *6*, 401–409. [[CrossRef](#)]
46. Dong, H. S-phase surface engineering of Fe-Cr, Co-Cr and Ni-Cr alloys. *Int. Mater. Rev.* **2010**, *55*, 65–98. [[CrossRef](#)]
47. Christiansen, T.L.; Somers, M.A.J. Low-temperature gaseous surface hardening of stainless steel: The current status. *Int. J. Mater. Res.* **2009**, *100*, 1361–1377. [[CrossRef](#)]
48. Collins, S.R.; Williams, P.C.; Marx, S.V.; Heuer, A.; Ernst, F.; Kahn, H. Low-Temperature Carburization of Austenitic Stainless Steels. In *ASM Handbook*; Dosset, J., Tottem, G.E., Eds.; ASM International: Materials Park, OH, USA, 2014; Volume 4D, pp. 451–460.
49. Scheuer, C.J.; Zanetti, F.I.; Cardoso, R.P.; Brunatto, S.F. Ultra-low—to high-temperature plasma-assisted nitriding: Revisiting and going further on the martensitic stainless steel treatment. *Mater. Res. Express* **2019**, *6*, 026529. [[CrossRef](#)]
50. Wriedt, H.A.; Gokcen, N.A.; Nafziger, R.H. The Fe-N (Iron-Nitrogen) system. *Bull. Alloy Phase Diagr.* **1987**, *8*, 355–377. [[CrossRef](#)]
51. Okamoto, H. The C-Fe (carbon-iron) system. *J. Phase Equilibria* **1992**, *13*, 543–565. [[CrossRef](#)]
52. Gavriljuk, V.G. Carbon and nitrogen in iron-based austenite and martensite: An attempt at comparative analysis. *J. Phys. IV Fr.* **2003**, *112*, 51–59. [[CrossRef](#)]
53. Shanina, B.D.; Gavriljuk, V.G.; Konchits, A.A.; Kolesnik, S.P. The influence of substitutional atoms upon the electron structure of the iron-based transition metal alloys. *J. Phys. Condens. Matter* **1998**, *10*, 1825–1838. [[CrossRef](#)]
54. Cao, Y.; Ernst, F.; Michal, G.M. Colossal carbon supersaturation in austenitic stainless steels carburized at low temperature. *Acta Mater.* **2003**, *51*, 4171–4181. [[CrossRef](#)]
55. Lengauer, W. Nitrides: Transition Metal Solid-state Chemistry. In *Encyclopedia of Inorganic and Bioinorganic Chemistry*; Scott, R.A., Ed.; John Wiley & Sons, Ltd.: Hoboken, NJ, USA, 2015; pp. 197–213. [[CrossRef](#)]
56. Shatynski, S.R. The thermochemistry of transition metal carbides. *Oxid. Met.* **1979**, *13*, 105–118. [[CrossRef](#)]
57. Williamson, D.L.; Ozturk, O.; Wei, R.; Wilbur, P.J. Metastable phase formation and enhanced diffusion in f.c.c. alloys under high dose, high flux nitrogen implantation at high and low ion energies. *Surf. Coat. Technol.* **1994**, *65*, 15–23. [[CrossRef](#)]

58. Christiansen, T.; Somers, M.A.J. Controlled dissolution of colossal quantities of nitrogen in stainless steel. *Metall. Mater. Trans. A* **2006**, *37*, 675–682. [[CrossRef](#)]
59. Christiansen, T.L.; Ståhl, K.; Brink, B.K.; Somers, M.A.J. On the Carbon Solubility in Expanded Austenite and Formation of Hägg Carbide in AISI 316 Stainless Steel. *Steel Res. Int.* **2016**, *87*, 1395–1405. [[CrossRef](#)]
60. Manova, D.; Thorwarth, G.; Mändl, S.; Neumann, H.; Stritzker, B.; Rauschenbach, B. Variable lattice expansion in martensitic stainless steel after nitrogen ion implantation. *Nucl. Instrum. Methods Phys. Res. Sect. B Beam Interact. Mater. At.* **2006**, *242*, 285–288. [[CrossRef](#)]
61. Michal, G.M.; Gu, X.; Jennings, W.D.; Kahn, H.; Ernst, F.; Heuer, A.H. Paraequilibrium Carburization of Duplex and Ferritic Stainless Steels. *Metall. Mater. Trans. A* **2009**, *40*, 1781–1790. [[CrossRef](#)]
62. Frandsen, R.B.; Christiansen, T.; Somers, M.A.J. Simultaneous surface engineering and bulk hardening of precipitation hardening stainless steel. *Surf. Coat. Technol.* **2006**, *200*, 5160–5169. [[CrossRef](#)]
63. Baniasadi, F.; Bahmannezhad, B.; Nikpoor, N.; Asgari, S. Thermal stability investigation of expanded martensite. *Surf. Coat. Technol.* **2016**, *300*, 87–94. [[CrossRef](#)]
64. Kim, S.K.; Yoo, J.S.; Priest, J.M.; Fewell, M.P. Characteristics of martensitic stainless steel nitrided in a low-pressure RF plasma. *Surf. Coat. Technol.* **2003**, *163–164*, 380–385. [[CrossRef](#)]
65. Brühl, S.P.; Charadia, R.; Simison, S.; Lamas, D.G.; Cabo, A. Corrosion behavior of martensitic and precipitation hardening stainless steels treated by plasma nitriding. *Surf. Coat. Technol.* **2010**, *204*, 3280–3286. [[CrossRef](#)]
66. Espitia, L.A.; Varela, L.; Pinedo, C.E.; Tschiptschin, A.P. Cavitation erosion resistance of low temperature plasma nitrided martensitic stainless steel. *Wear* **2013**, *301*, 449–456. [[CrossRef](#)]
67. Espitia, L.A.; Dong, H.; Li, X.-Y.; Pinedo, C.E.; Tschiptschin, A.P. Cavitation erosion resistance and wear mechanisms of active screen low temperature plasma nitrided AISI 410 martensitic stainless steel. *Wear* **2015**, *332–333*, 1070–1079. [[CrossRef](#)]
68. Wang, J.; Lin, Y.; Zeng, D.; Yan, J.; Fan, H. Effects of the Process Parameters on the Microstructure and Properties of Nitrided 17–4PH Stainless Steel. *Metall. Mater. Trans. B* **2013**, *44*, 414–422. [[CrossRef](#)]
69. Bottoli, F.; Winther, G.; Christiansen, T.L.; Somers, M.A.J. Influence of Microstructure and Process Conditions on Simultaneous Low-Temperature Surface Hardening and Bulk Precipitation Hardening of Nanoflex[®]. *Metall. Mater. Trans. A* **2015**, *46*, 5201–5216. [[CrossRef](#)]
70. Pinedo, C.E.; Larrotta, S.I.V.; Nishikawa, A.S.; Dong, H.; Li, X.-Y.; Magnabosco, R.; Tschiptschin, A.P. Low temperature active screen plasma nitriding of 17–4 PH stainless steel. *Surf. Coat. Technol.* **2016**, *308*, 189–194. [[CrossRef](#)]
71. Dong, H.; Esfandiari, M.; Li, X.Y. On the microstructure and phase identification of plasma nitrided 17–4PH precipitation hardening stainless steel. *Surf. Coat. Technol.* **2008**, *202*, 2969–2975. [[CrossRef](#)]
72. Somers, M.A.J.; Lankreijer, R.M.; Mittemeijer, E.J. Excess nitrogen in the ferrite matrix of nitrided binary iron-based alloys. *Philos. Mag. A* **1989**, *59*, 353–378. [[CrossRef](#)]
73. Pinedo, C.E.; Monteiro, W.A. On the kinetics of plasma nitriding a martensitic stainless steel type AISI 420. *Surf. Coat. Technol.* **2004**, *179*, 119–123. [[CrossRef](#)]
74. Li, C.X.; Bell, T. A comparative study of low temperature plasma nitriding, carburising and nitrocarburising of AISI 410 martensitic stainless steel. *Mater. Sci. Technol.* **2007**, *23*, 355–361. [[CrossRef](#)]
75. Barua, A.; Kim, H.; Lee, I. Effect of the amount of CH₄ gas on the characteristics of surface layers of low temperature plasma nitrided martensitic precipitation-hardening stainless steel. *Surf. Coat. Technol.* **2016**, *307*, 1034–1040. [[CrossRef](#)]
76. Mändl, S.; Fritzsche, B.; Manova, D.; Hirsch, D.; Neumann, H.; Richter, E.; Rauschenbach, B. Wear reduction in AISI 630 martensitic stainless steel after energetic nitrogen ion implantation. *Surf. Coat. Technol.* **2005**, *195*, 258–263. [[CrossRef](#)]
77. Scheuer, C.J.; Cardoso, R.P.; Zanetti, F.I.; Amaral, T.; Brunatto, S.F. Low-temperature plasma carburizing of AISI 420 martensitic stainless steel: Influence of gas mixture and gas flow rate. *Surf. Coat. Technol.* **2012**, *206*, 5085–5090. [[CrossRef](#)]
78. Scheuer, C.J.; Cardoso, R.P.; Brunatto, S.F. Sequential low-temperature plasma-assisted thermochemical treatments of the AISI 420 martensitic stainless steel. *Surf. Coat. Technol.* **2021**, *421*, 127459. [[CrossRef](#)]
79. Scheuer, C.J.; Cardoso, R.P.; Brunatto, S.F. Low-temperature Plasma Assisted Thermochemical Treatments of AISI 420 Steel: Comparative Study of Obtained Layers. *Mater. Res.* **2015**, *18*, 1392–1399. [[CrossRef](#)]
80. Anjos, A.D.; Scheuer, C.J.; Brunatto, S.F.; Cardoso, R.P. Low-temperature plasma nitrocarburizing of the AISI 420 martensitic stainless steel: Microstructure and process kinetics. *Surf. Coat. Technol.* **2015**, *275*, 51–57. [[CrossRef](#)]
81. Scheuer, C.J.; Cardoso, R.P.; Mafra, M.; Brunatto, S.F. AISI 420 martensitic stainless steel low-temperature plasma assisted carburizing kinetics. *Surf. Coat. Technol.* **2013**, *214*, 30–37. [[CrossRef](#)]
82. Scheuer, C.J.; Possoli, F.A.A.; Borges, P.C.; Cardoso, R.P.; Brunatto, S.F. AISI 420 martensitic stainless steel corrosion resistance enhancement by low-temperature plasma carburizing. *Electrochim. Acta* **2019**, *317*, 70–82. [[CrossRef](#)]
83. Fernandes, F.A.P.; Picone, C.A.; Totten, G.E.; Casteletti, L.C. Corrosion Behavior of Plasma Nitrided and Nitrocarburised Supermartensitic Stainless Steel. *Mater. Res.* **2018**, *21*, e20160793. [[CrossRef](#)]
84. Cheng, Z.; Li, C.X.; Dong, H.; Bell, T. Low temperature plasma nitrocarburising of AISI 316 austenitic stainless steel. *Surf. Coat. Technol.* **2005**, *191*, 195–200. [[CrossRef](#)]
85. Ferreira, L.M.; Brunatto, S.F.; Cardoso, R.P. Martensitic Stainless Steels Low-temperature Nitriding: Dependence of Substrate Composition. *Mater. Res.* **2015**, *18*, 622–627. [[CrossRef](#)]

86. Figueroa, C.A.; Alvarez, F.; Mitchell, D.R.G.; Collins, G.A.; Short, K.T. Previous heat treatment inducing different plasma nitriding behaviors in martensitic stainless steels. *J. Vac. Sci. Technol. A* **2006**, *24*, 1795–1801. [[CrossRef](#)]
87. Riazzi, H.; Ashrafizadeh, F.; Hosseini, S.R.; Ghomashchi, R.; Liu, R. Characterization of simultaneous aged and plasma nitrided 17–4 PH stainless steel. *Mater. Charact.* **2017**, *133*, 33–43. [[CrossRef](#)]
88. Manova, D.; Mändl, S.; Neumann, H.; Rauschenbach, B. Influence of annealing conditions on ion nitriding of martensitic stainless steel. *Surf. Coat. Technol.* **2006**, *200*, 6563–6567. [[CrossRef](#)]
89. Sun, Y.; Bell, T. Low Temperature Plasma Nitriding Characteristics of Precipitation Hardening Stainless Steel. *Surf. Eng.* **2003**, *19*, 331–336. [[CrossRef](#)]
90. Manova, D.; Mändl, S.; Neumann, H.; Rauschenbach, B. Wear behaviour of martensitic stainless steel after PIII surface treatment. *Surf. Coat. Technol.* **2005**, *200*, 137–140. [[CrossRef](#)]
91. Borgioli, F.; Fossati, A.; Rauegi, L.; Galvanetto, E.; Bacci, T. Low temperature glow-discharge nitriding of stainless steels. In Proceedings of the 7th European Stainless Steel Conference: Science and Market, Como, Italy, 21–23 September 2011; Associazione Italiana di Metallurgia: Milan, Italy, 2011.
92. Brunatto, S.F.; Scheuer, C.J.; Boromei, I.; Martini, C.; Ceschini, L.; Cardoso, R.P. Martensite coarsening in low-temperature plasma carburizing. *Surf. Coat. Technol.* **2018**, *350*, 161–171. [[CrossRef](#)]
93. Figueroa, C.A.; Alvarez, F.; Zhang, Z.; Collins, G.A.; Short, K.T. Structural modifications and corrosion behavior of martensitic stainless steel nitrided by plasma immersion ion implantation. *J. Vac. Sci. Technol. A* **2005**, *23*, 693–698. [[CrossRef](#)]
94. Kurelo, B.C.E.S.; de Souza, G.B.; Serbena, F.C.; de Oliveira, W.R.; Marino, C.E.B.; Taminato, L.A. Performance of nitrogen ion-implanted supermartensitic stainless steel in chlorine- and hydrogen-rich environments. *Surf. Coat. Technol.* **2018**, *351*, 29–41. [[CrossRef](#)]
95. Allenstein, A.N.; Cardoso, R.P.; Machado, K.D.; Weber, S.; Pereira, K.M.P.; dos Santos, C.A.L.; Panossian, Z.; Buschinelli, A.J.A.; Brunatto, S.F. Strong evidences of tempered martensite-to-nitrogen-expanded austenite transformation in CA-6NM steel. *Mater. Sci. Eng. A* **2012**, *552*, 569–572. [[CrossRef](#)]
96. Zangiabadi, A. Low-Temperature Interstitial Hardening of 15-5 Precipitation Hardening Martensitic Stainless Steel. Ph.D. Thesis, Department of Materials Science and Engineering, Case Western Reserve University, Cleveland, OH, USA, 2016.
97. Zangiabadi, A.; Dalton, J.C.; Wang, D.; Ernst, F.; Heuer, A.H. The Formation of Martensitic Austenite During Nitridation of Martensitic and Duplex Stainless Steels. *Metall. Mater. Trans. A* **2017**, *48*, 8–13. [[CrossRef](#)]
98. Maugis, P.; Connétable, D.; Eyméoud, P. Stability of Zener order in martensite: An atomistic evidence. *Scr. Mater.* **2021**, *194*, 113632. [[CrossRef](#)]
99. Tanaka, T.; Maruyama, N.; Nakamura, N.; Wilkinson, A.J. Tetragonality of Fe-C martensite—A pattern matching electron backscatter diffraction analysis compared to X-ray diffraction. *Acta Mater.* **2020**, *195*, 728–738. [[CrossRef](#)]
100. Tsuchiyama, T.; Inoue, K.; Hyodo, K.; Akama, D.; Nakada, N.; Takaki, S.; Koyano, T. Comparison of Microstructure and Hardness between High-carbon and High-nitrogen Martensites. *ISIJ Int.* **2019**, *59*, 161–168. [[CrossRef](#)]
101. Siqueira, J.S.; de Abreu Alves, M.R.; Marcial Luiz, T.; Renzetti, R.A. Effect of heat treatment on the chromium-depleted zones of a high carbon martensitic stainless steel. *Mater. Corros.* **2021**, *72*, 1752–1761. [[CrossRef](#)]
102. Mändl, S.; Rauschenbach, B. Comparison of expanded austenite and expanded martensite formed after nitrogen PIII. *Surf. Coat. Technol.* **2004**, *186*, 277–281. [[CrossRef](#)]
103. Borgioli, F.; Fossati, A.; Galvanetto, E.; Bacci, T.; Pradelli, G. Glow discharge nitriding of AISI 316L austenitic stainless steel: Influence of treatment pressure. *Surf. Coat. Technol.* **2006**, *200*, 5505–5513. [[CrossRef](#)]
104. Luiz, L.A.; Kurelo, B.C.E.S.; de Souza, G.B.; de Andrade, J.; Marino, C.E.B. Effect of nitrogen plasma immersion ion implantation on the corrosion protection mechanisms of different stainless steels. *Mater. Today Commun.* **2021**, *28*, 102655. [[CrossRef](#)]
105. Liu, R.L.; Yan, F.; Wei, C.Y.; Yan, M.F. Characteristics of carbon-expanded α phase layer on AISI 431 stainless steel using experimental and first-principles calculation methods. *Surf. Coat. Technol.* **2019**, *375*, 66–73. [[CrossRef](#)]
106. Li, C.X.; Bell, T. Corrosion properties of plasma nitrided AISI 410 martensitic stainless steel in 3.5% NaCl and 1% HCl aqueous solutions. *Corros. Sci.* **2006**, *48*, 2036–2049. [[CrossRef](#)]
107. Rovani, A.C.; Breganon, R.; de Souza, G.S.; Brunatto, S.F.; Pintaúde, G. Scratch resistance of low-temperature plasma nitrided and carburized martensitic stainless steel. *Wear* **2017**, *376–377*, 70–76. [[CrossRef](#)]
108. Nakasa, K.; Yamamoto, A.; Wang, R.; Sumomogi, T. Effect of plasma nitriding on the strength of fine protrusions formed by sputter etching of AISI type 420 stainless steel. *Surf. Coat. Technol.* **2015**, *272*, 298–308. [[CrossRef](#)]
109. Xi, Y.; Liu, D.; Han, D. Improvement of erosion and erosion–corrosion resistance of AISI420 stainless steel by low temperature plasma nitriding. *Appl. Surf. Sci.* **2008**, *254*, 5953–5958. [[CrossRef](#)]
110. Corengia, P.; Walther, F.; Ybarra, G.; Sommadossi, S.; Corbari, R.; Broitman, E. Friction and rolling–sliding wear of DC-pulsed plasma nitrided AISI 410 martensitic stainless steel. *Wear* **2006**, *260*, 479–485. [[CrossRef](#)]
111. Bernardelli, E.A.; Borges, P.C.; Fontana, L.C.; Floriano, J.B. Role of plasma nitriding temperature and time in the corrosion behaviour and microstructure evolution of 15–5 PH stainless steel. *Kov. Mater.* **2010**, *48*, 110–115. [[CrossRef](#)]
112. Blawert, C.; Mordike, B.L.; Jirásková, Y.; Schneeweiss, O. Structure and composition of expanded austenite produced by nitrogen plasma immersion ion implantation of stainless steels X6CrNiTi1810 and X2CrNiMoN2253. *Surf. Coat. Technol.* **1999**, *116–119*, 189–198. [[CrossRef](#)]

113. Kurelo, B.C.E.S.; de Souza, G.B.; Serbena, F.C.; Lepienski, C.M.; Borges, P.C. Mechanical properties and corrosion resistance of α_N -rich layers produced by PIII on a super ferritic stainless steel. *Surf. Coat. Technol.* **2020**, *403*, 126388. [[CrossRef](#)]
114. Alphonsa, J.; Mukherjee, S.; Raja, V.S. Study of plasma nitriding and nitrocarburising of AISI 430F stainless steel for high hardness and corrosion resistance. *Corros. Eng. Sci. Technol.* **2018**, *53*, 51–58. [[CrossRef](#)]
115. de Sousa, R.R.M.; de Araújo, F.O.; da Costa, J.A.P.; de Oliverira, A.M.; Melo, M.S.; Alves, C., Jr. Cathodic Cage Nitriding of AISI 409 Ferritic Stainless Steel with the Addition of CH_4 . *Mater. Res.* **2012**, *15*, 260–265. [[CrossRef](#)]
116. Larisch, B.; Brusky, U.; Spies, H.-J. Plasma nitriding of stainless steels at low temperatures. *Surf. Coat. Technol.* **1999**, *116–119*, 205–211. [[CrossRef](#)]
117. Feugeas, J.; Gómez, B.; Craievich, A. Ion nitriding of stainless steels. Real time surface characterization by synchrotron X-ray diffraction. *Surf. Coat. Technol.* **2002**, *154*, 167–175. [[CrossRef](#)]
118. Blawert, C.; Mordike, B.L.; Rensch, U.; Wunsch, R.; Wiedemann, R.; Oettel, H. Influence of the material composition on the nitriding result of steels by plasma immersion ion implantation. *Surf. Coat. Technol.* **2000**, *131*, 334–339. [[CrossRef](#)]
119. Schreiber, G.; Rensch, U.; Oettel, H.; Blawert, C.; Mordike, B.L. Thermal stability of P^{I^3} nitrided surface layers on ferritic steels. *Surf. Coat. Technol.* **2003**, *169–170*, 447–451. [[CrossRef](#)]
120. Spies, H.-J. Corrosion Behaviour of Nitrided, nitrocarburised and Carburised Steels. In *Thermochemical Surface Engineering of Steel*; Mittemeijer, E.J., Somers, M.A.J., Eds.; Woodhead Publishing: Oxford, UK, 2015; pp. 267–309, ISBN 9780857095923. [[CrossRef](#)]
121. Kliauga, A.M.; Pohl, M.; Cordier-Robert, C.; Foct, J. Phase transformations in a super ferritic stainless steel containing 28% Cr after nitrogen ion implantation. *J. Mater. Sci.* **1999**, *34*, 4065–4073. [[CrossRef](#)]
122. Jirásková, Y.; Blawert, C.; Schneeweiss, O. Thermal Stability of Stainless Steel Surfaces Nitrided by Plasma Immersion Ion Implantation. *Phys. Status Solidi* **1999**, *175*, 537–548. [[CrossRef](#)]
123. de Araújo Junior, E.; Bandeira, R.M.; Manfrinato, M.D.; Moreto, J.A.; Borges, R.; dos Santos Vales, S.; Suzuki, P.A.; Rossino, L.S. Effect of ionic plasma nitriding process on the corrosion and micro-abrasive wear behavior of AISI 316L austenitic and AISI 470 super-ferritic stainless steels. *J. Mater. Res. Technol.* **2019**, *8*, 2180–2191. [[CrossRef](#)]
124. Tuckart, W.; Gregorio, M.; Iurman, L. Sliding wear of plasma nitrided AISI 405 ferritic stainless steel. *Surf. Eng.* **2010**, *26*, 185–190. [[CrossRef](#)]
125. Bielawski, J.; Baranowska, J.; Szczecinski, K. Microstructure and properties of layers on chromium steel. *Surf. Coat. Technol.* **2006**, *200*, 6572–6577. [[CrossRef](#)]
126. Michler, T.; Grischke, M.; Bewilogua, K.; Dimigen, H. Properties of duplex coatings prepared by plasma nitriding and PVD Ti-C:H deposition on X20Cr13 ferritic stainless steel. *Thin Solid Film.* **1998**, *322*, 206–212. [[CrossRef](#)]
127. Spies, H.-J.; Eckstein, C.; Zimdars, H. Structure and corrosion behaviour of stainless steels after plasma and gas nitriding. *Surf. Eng.* **2002**, *18*, 459–460. [[CrossRef](#)]
128. Gontijo, L.C.; Machado, R.; Casteletti, L.C.; Kuri, S.E.; Nascente, P.A.P. X-ray diffraction characterisation of expanded austenite and ferrite in plasma nitrided stainless steels. *Surf. Eng.* **2010**, *26*, 265–270. [[CrossRef](#)]
129. Bielawski, J.; Baranowska, J. Formation of nitrided layers on duplex steel—Influence of multiphase substrate. *Surf. Eng.* **2010**, *26*, 299–304. [[CrossRef](#)]
130. Pinedo, C.E.; Varela, L.B.; Tschiptschin, A.P. Low-temperature plasma nitriding of AISI F51 duplex stainless steel. *Surf. Coat. Technol.* **2013**, *232*, 839–843. [[CrossRef](#)]
131. Chiu, L.H.; Su, Y.Y.; Chen, F.S.; Chang, H. Microstructure and Properties of Active Screen Plasma Nitrided Duplex Stainless Steel. *Mater. Manuf. Process.* **2010**, *25*, 316–323. [[CrossRef](#)]
132. Tschiptschin, A.P.; Varela, L.B.; Pinedo, C.E.; Li, X.Y.; Dong, H. Development and microstructure characterization of single and duplex nitriding of UNS S31803 duplex stainless steel. *Surf. Coat. Technol.* **2017**, *327*, 83–92. [[CrossRef](#)]
133. de Oliveira, W.R.; Kurelo, B.C.E.S.; Ditzel, D.G.; Serbena, F.C.; Foerster, C.E.; de Souza, G.B. On the S-phase formation and the balanced plasma nitriding of austenitic-ferritic super duplex stainless steel. *Appl. Surf. Sci.* **2018**, *434*, 1161–1174. [[CrossRef](#)]
134. Christiansen, T.; Somers, M.A.J. Low temperature gaseous nitriding and carburising of stainless steel. *Surf. Eng.* **2005**, *21*, 445–455. [[CrossRef](#)]
135. Blawert, C.; Weisheit, A.; Mordike, B.L.; Knoop, R.M. Plasma immersion ion implantation of stainless steel: Austenitic stainless steel in comparison to austenitic-ferritic stainless steel. *Surf. Coat. Technol.* **1996**, *85*, 15–27. [[CrossRef](#)]
136. Calabokis, O.P.; de la Rosa, Y.N.; Lepienski, C.M.; Cardoso, R.P.; Borges, P.C. Crevice and pitting corrosion of low temperature plasma nitrided UNS S32750 super duplex stainless steel. *Surf. Coat. Technol.* **2021**, *413*, 127095. [[CrossRef](#)]
137. Pinedo, C.E.; Tschiptschin, A.P. Low temperature plasma carburizing of AISI 316L austenitic stainless steel and AISI F51 duplex stainless steel. *Rev. Esc. Minas* **2013**, *66*, 209–214. [[CrossRef](#)]
138. Alphonsa, J.; Raja, V.S.; Mukherjee, S. Study of plasma nitriding and nitrocarburizing for higher corrosion resistance and hardness of 2205 duplex stainless steel. *Corros. Sci.* **2015**, *100*, 121–132. [[CrossRef](#)]
139. Bobadilla, M.; Tschiptschin, A.P. On the Nitrogen Diffusion in a Duplex Stainless Steel. *Mater. Res.* **2015**, *18*, 390–394. [[CrossRef](#)]
140. Dalton, J.C.; Ernst, F.; Heuer, A.H. Low-Temperature Nitridation of 2205 Duplex Stainless Steel. *Metall. Mater. Trans. A* **2020**, *51*, 608–617. [[CrossRef](#)]
141. Wang, D.; Chen, C.-W.; Dalton, J.C.; Yang, F.; Sharghi-Moshtaghin, R.; Kahn, H.; Ernst, F.; Williams, R.E.A.; McComb, D.W.; Heuer, A.H. “Colossal” interstitial supersaturation in delta ferrite in stainless steels—I. Low-temperature carburization. *Acta Mater.* **2015**, *86*, 193–207. [[CrossRef](#)]

142. Sasidhar, K.N.; Meka, S.R. What causes the colossal C supersaturation of δ -ferrite in stainless steel during low-temperature carburization? *Scr. Mater.* **2019**, *162*, 118–120. [[CrossRef](#)]
143. Pintaude, G.; Rovani, A.C.; das Neves, J.C.K.; Lagoeiro, L.E.; Li, X.; Dong, H.S. Wear and Corrosion Resistances of Active Screen Plasma-Nitrided Duplex Stainless Steels. *J. Mater. Eng. Perform.* **2019**, *28*, 3673–3682. [[CrossRef](#)]
144. Kahn, H.; Heuer, A.H.; Michal, G.M.; Ernst, F.; Sharghi-Moshtaghin, R.; Ge, Y.; Natishan, P.M.; Rayne, R.J.; Martin, F.J. Interstitial hardening of duplex 2205 stainless steel by low temperature carburisation: Enhanced mechanical and electrochemical performance. *Surf. Eng.* **2012**, *28*, 213–219. [[CrossRef](#)]
145. Hannula, S.-P.; Nenonen, P.; Hirvonen, J.-P. Surface structure and properties of ion-nitrided austenitic stainless steels. *Thin Solid Film.* **1989**, *181*, 343–350. [[CrossRef](#)]
146. Adachi, S.; Yamaguchi, T.; Ueda, N. Formation and Properties of Nitrocarburizing S-Phase on AISI 316L Stainless Steel-Based WC Composite Layers by Low-Temperature Plasma Nitriding. *Metals* **2021**, *11*, 1538. [[CrossRef](#)]
147. Adachi, S.; Ueda, N. Combined plasma carburizing and nitriding of sprayed AISI 316L steel coating for improved wear resistance. *Surf. Coat. Technol.* **2014**, *259*, 44–49. [[CrossRef](#)]
148. Adachi, S.; Egawa, M.; Yamaguchi, T.; Ueda, N. Low-Temperature Plasma Nitriding for Austenitic Stainless Steel Layers with Various Nickel Contents Fabricated via Direct Laser Metal Deposition. *Coatings* **2020**, *10*, 365. [[CrossRef](#)]
149. Adachi, S.; Ueda, N. Wear and Corrosion Properties of Cold-Sprayed AISI 316L Coatings Treated by Combined Plasma Carburizing and Nitriding at Low Temperature. *Coatings* **2018**, *8*, 456. [[CrossRef](#)]
150. Adachi, S.; Ueda, N. Formation of Expanded Austenite on a Cold-Sprayed AISI 316L Coating by Low-Temperature Plasma Nitriding. *J. Therm. Spray Technol.* **2015**, *24*, 1399–1407. [[CrossRef](#)]
151. Adachi, S.; Ueda, N. Formation of S-phase layer on plasma sprayed AISI 316L stainless steel coating by plasma nitriding at low temperature. *Thin Solid Film.* **2012**, *523*, 11–14. [[CrossRef](#)]
152. Lindner, T.; Mehner, T.; Lampke, T. Surface modification of austenitic thermal-spray coatings by low-temperature nitrocarburizing. *IOP Conf. Ser. Mater. Sci. Eng.* **2016**, *118*, 12008. [[CrossRef](#)]
153. Lindner, T.; Kutschmann, P.; Löbel, M.; Lampke, T. Hardening of HVOF-Sprayed Austenitic Stainless-Steel Coatings by Gas Nitriding. *Coatings* **2018**, *8*, 348. [[CrossRef](#)]
154. Kutschmann, P.; Lindner, T.; Börner, K.; Reese, U.; Lampke, T. Effect of Adjusted Gas Nitriding Parameters on Microstructure and Wear Resistance of HVOF-Sprayed AISI 316L Coatings. *Materials* **2019**, *12*, 1760. [[CrossRef](#)]
155. Esfandiari, M.; Dong, H. Plasma surface engineering of precipitation hardening stainless steels. *Surf. Eng.* **2006**, *22*, 86–92. [[CrossRef](#)]
156. Esfandiari, M.; Dong, H. Improving the surface properties of A286 precipitation-hardening stainless steel by low-temperature plasma nitriding. *Surf. Coat. Technol.* **2007**, *201*, 6189–6196. [[CrossRef](#)]
157. Wang, S.; Cai, W.; Li, J.; Wei, W.; Hu, J. A novel rapid D.C. plasma nitriding at low gas pressure for 304 austenitic stainless steel. *Mater. Lett.* **2013**, *105*, 47–49. [[CrossRef](#)]
158. Lu, S.; Zhao, X.; Wang, S.; Li, J.; Wei, W.; Hu, J. Performance enhancement by plasma nitriding at low gas pressure for 304 austenitic stainless steel. *Vacuum* **2017**, *145*, 334–339. [[CrossRef](#)]
159. Buhagiar, J.; Li, X.; Dong, H. Formation and microstructural characterisation of S-phase layers in Ni-free austenitic stainless steels by low-temperature plasma surface alloying. *Surf. Coat. Technol.* **2009**, *204*, 330–335. [[CrossRef](#)]
160. Borgioli, F.; Fossati, A.; Matassini, G.; Galvanetto, E.; Bacci, T. Low temperature glow-discharge nitriding of a low nickel austenitic stainless steel. *Surf. Coat. Technol.* **2010**, *204*, 3410–3417. [[CrossRef](#)]
161. Borgioli, F.; Galvanetto, E.; Bacci, T. Surface Modification of a Nickel-Free Austenitic Stainless Steel by Low-Temperature Nitriding. *Metals* **2021**, *11*, 1845. [[CrossRef](#)]
162. Tao, X.; Li, X.; Dong, H.; Matthews, A.; Leyland, A. Evaluation of the sliding wear and corrosion performance of triode-plasma nitrided Fe-17Cr-20Mn-0.5N high-manganese and Fe-19Cr-35Ni-1.2Si high-nickel austenitic stainless steels. *Surf. Coat. Technol.* **2021**, *409*, 126890. [[CrossRef](#)]
163. Ernst, F.; Avishai, A.; Kahn, H.; Gu, X.; Michal, G.M.; Heuer, A.H. Enhanced Carbon Diffusion in Austenitic Stainless Steel Carburized at Low Temperature. *Metall. Mater. Trans. A* **2009**, *40*, 1768–1780. [[CrossRef](#)]
164. Wu, D.; Ge, Y.; Kahn, H.; Ernst, F.; Heuer, A.H. Diffusion profiles after nitrocarburizing austenitic stainless steel. *Surf. Coat. Technol.* **2015**, *279*, 180–185. [[CrossRef](#)]
165. Mändl, S.; Scholze, F.; Neumann, H.; Rauschenbach, B. Nitrogen diffusivity in expanded austenite. *Surf. Coat. Technol.* **2003**, *174–175*, 1191–1195. [[CrossRef](#)]
166. Williamson, D.L.; Ivanov, I.; Wei, R.; Wilbur, P.J. Role of Chromium in High-Dose, High-Rate, Elevated Temperature Nitrogen Implantation of Austenitic Stainless Steels. *MRS Proc.* **1991**, *235*, 473. [[CrossRef](#)]
167. Parascandola, S.; Günzel, R.; Grötzschel, R.; Richter, E.; Möller, W. Analysis of deuterium induced nuclear reactions giving criteria for the formation process of expanded austenite. *Nucl. Instrum. Methods Phys. Res. Sect. B Beam Interact. Mater. At.* **1998**, *136–138*, 1281–1285. [[CrossRef](#)]
168. Christiansen, T.L.; Drouet, M.; Martinavičius, A.; Somers, M.A.J. Isotope exchange investigation of nitrogen redistribution in expanded austenite. *Scr. Mater.* **2013**, *69*, 582–585. [[CrossRef](#)]
169. Christiansen, T.; Dahl, K.V.; Somers, M.A.J. Nitrogen diffusion and nitrogen depth profiles in expanded austenite: Experimental assessment, numerical simulation and role of stress. *Mater. Sci. Technol.* **2008**, *24*, 159–167. [[CrossRef](#)]

170. Jespersen, F.N.; Hattel, J.H.; Somers, M.A.J. Modelling the evolution of composition-and stress-depth profiles in austenitic stainless steels during low-temperature nitriding. *Model. Simul. Mater. Sci. Eng.* **2016**, *24*, 25003. [[CrossRef](#)]
171. Galdikas, A.; Moskaliuviene, T. The Anisotropic Stress-Induced Diffusion and Trapping of Nitrogen in Austenitic Stainless Steel during Nitriding. *Metals* **2020**, *10*, 1319. [[CrossRef](#)]
172. Li, X.Y. Low Temperature Plasma Nitriding of 316 Stainless Steel—Nature of S Phase and Its Thermal Stability. *Surf. Eng.* **2001**, *17*, 147–152. [[CrossRef](#)]
173. Li, X.Y.; Thaiwatthana, S.; Dong, H.; Bell, T. Thermal stability of carbon S phase in 316 stainless steel. *Surf. Eng.* **2002**, *18*, 448–451. [[CrossRef](#)]
174. Borgioli, F.; Galvanetto, E.; Bacci, T. Corrosion behaviour of low temperature nitrided nickel-free, AISI 200 and AISI 300 series austenitic stainless steels in NaCl solution. *Corros. Sci.* **2018**, *136*, 352–365. [[CrossRef](#)]
175. Borgioli, F.; Galvanetto, E.; Bacci, T. Influence of surface morphology and roughness on water wetting properties of low temperature nitrided austenitic stainless steels. *Mater. Charact.* **2014**, *95*, 278–284. [[CrossRef](#)]
176. Tao, X.; Liu, X.; Matthews, A.; Leyland, A. The influence of stacking fault energy on plasticity mechanisms in triode-plasma nitrided austenitic stainless steels: Implications for the structure and stability of nitrogen-expanded austenite. *Acta Mater.* **2019**, *164*, 60–75. [[CrossRef](#)]
177. Baranowska, J.; Arnold, B. Corrosion resistance of nitrided layers on austenitic steel. *Surf. Coat. Technol.* **2006**, *200*, 6623–6628. [[CrossRef](#)]
178. Borgioli, F.; Fossati, A.; Galvanetto, E.; Bacci, T. Glow-discharge nitriding of AISI 316L austenitic stainless steel: Influence of treatment temperature. *Surf. Coat. Technol.* **2005**, *200*, 2474–2480. [[CrossRef](#)]
179. Wu, D.; Kahn, H.; Dalton, J.C.; Michal, G.M.; Ernst, F.; Heuer, A.H. Orientation dependence of nitrogen supersaturation in austenitic stainless steel during low-temperature gas-phase nitriding. *Acta Mater.* **2014**, *79*, 339–350. [[CrossRef](#)]
180. Templier, C.; Stinville, J.C.; Villechaise, P.; Renault, P.O.; Abrasonis, G.; Rivière, J.P.; Martinavičius, A.; Drouet, M. On lattice plane rotation and crystallographic structure of the expanded austenite in plasma nitrided AISI 316L steel. *Surf. Coat. Technol.* **2010**, *204*, 2551–2558. [[CrossRef](#)]
181. Borgioli, F.; Galvanetto, E.; Bacci, T. Low temperature nitriding of AISI 300 and 200 series austenitic stainless steels. *Vacuum* **2016**, *127*, 51–60. [[CrossRef](#)]
182. Lei, M.K. Phase transformations in plasma source ion nitrided austenitic stainless steel at low temperature. *J. Mater. Sci.* **1999**, *34*, 5975–5982. [[CrossRef](#)]
183. Yakubtsov, I.A.; Ariapour, A.; Perovic, D.D. Effect of nitrogen on stacking fault energy of f.c.c. iron-based alloys. *Acta Mater.* **1999**, *47*, 1271–1279. [[CrossRef](#)]
184. Talonen, J.; Hänninen, H. Formation of shear bands and strain-induced martensite during plastic deformation of metastable austenitic stainless steels. *Acta Mater.* **2007**, *55*, 6108–6118. [[CrossRef](#)]
185. Tao, X.; Qi, J.; Rainforth, M.; Matthews, A.; Leyland, A. On the interstitial induced lattice inhomogeneities in nitrogen-expanded austenite. *Scr. Mater.* **2020**, *185*, 146–151. [[CrossRef](#)]
186. Tong, K.; Ye, F.; Che, H.; Lei, M.K.; Miao, S.; Zhang, C. High-density stacking faults in a supersaturated nitrided layer on austenitic stainless steel. *J. Appl. Crystallogr.* **2016**, *49*, 1967–1971. [[CrossRef](#)]
187. Lei, M.K.; Huang, Y.; Zhang, Z.L. In situ Transformation of Nitrogen-induced h.c.p. Martensite in Plasma Source Ion–nitrided Austenitic Stainless Steel. *J. Mater. Sci. Lett.* **1998**, *17*, 1165–1167. [[CrossRef](#)]
188. Tsujikawa, M.; Yamauchi, N.; Ueda, N.; Sone, T.; Hirose, Y. Behavior of carbon in low temperature plasma nitriding layer of austenitic stainless steel. *Surf. Coat. Technol.* **2005**, *193*, 309–313. [[CrossRef](#)]
189. Williamson, D.L.; Davis, J.A.; Wilbur, P.J. Effect of austenitic stainless steel composition on low-energy, high-flux, nitrogen ion beam processing. *Surf. Coat. Technol.* **1998**, *103–104*, 178–184. [[CrossRef](#)]
190. Sun, Y. Hybrid plasma surface alloying of austenitic stainless steels with nitrogen and carbon. *Mater. Sci. Eng. A* **2005**, *404*, 124–129. [[CrossRef](#)]
191. Tsujikawa, M.; Yoshida, D.; Yamauchi, N.; Ueda, N.; Sone, T.; Tanaka, S. Surface material design of 316 stainless steel by combination of low temperature carburizing and nitriding. *Surf. Coat. Technol.* **2005**, *200*, 507–511. [[CrossRef](#)]
192. Niu, W.; Lillard, R.S.; Li, Z.; Ernst, F. Properties of the Passive Film Formed on Interstitially Hardened AISI 316L Stainless Steel. *Electrochim. Acta* **2015**, *176*, 410–419. [[CrossRef](#)]
193. Sun, Y. Corrosion behaviour of low temperature plasma carburised 316L stainless steel in chloride containing solutions. *Corros. Sci.* **2010**, *52*, 2661–2670. [[CrossRef](#)]
194. Czerwiec, T.; Andrieux, A.; Marcos, G.; Michel, H.; Bauer, P. Is “expanded austenite” really a solid solution? Mössbauer observation of an annealed AISI 316L nitrided sample. *J. Alloy. Compd.* **2019**, *811*, 151972. [[CrossRef](#)]
195. Stróż, D.; Psoda, M. TEM studies of plasma nitrided austenitic stainless steel. *J. Microsc.* **2010**, *237*, 227–231. [[CrossRef](#)]
196. Jiang, J.C.; Meletis, E.I. Microstructure of the nitride layer of AISI 316 stainless steel produced by intensified plasma assisted processing. *J. Appl. Phys.* **2000**, *88*, 4026–4031. [[CrossRef](#)]
197. Blawert, C.; Kalvelage, H.; Mordike, B.L.; Collins, G.A.; Short, K.T.; Jirásková, Y.; Schneeweiss, O. Nitrogen and carbon expanded austenite produced by P^3 . *Surf. Coat. Technol.* **2001**, *136*, 181–187. [[CrossRef](#)]
198. Fewell, M.P.; Priest, J.M. High-order diffractometry of expanded austenite using synchrotron radiation. *Surf. Coat. Technol.* **2008**, *202*, 1802–1815. [[CrossRef](#)]

199. Liang, W.; Xiaolei, X.; Jiujun, X.; Yaqin, S. Characteristics of low pressure plasma arc source ion nitrided layer on austenitic stainless steel at low temperature. *Thin Solid Film.* **2001**, *391*, 11–16. [[CrossRef](#)]
200. Riviere, J.P.; Cahoreau, M.; Meheust, P. Chemical bonding of nitrogen in low energy high flux implanted austenitic stainless steel. *J. Appl. Phys.* **2002**, *91*, 6361–6366. [[CrossRef](#)]
201. Martinavičius, A.; Abrasonis, G.; Scheinost, A.C.; Danoix, R.; Danoix, F.; Stinville, J.C.; Talut, G.; Templier, C.; Liedke, O.; Gemming, S.; et al. Nitrogen interstitial diffusion induced decomposition in AISI 304L austenitic stainless steel. *Acta Mater.* **2012**, *60*, 4065–4076. [[CrossRef](#)]
202. Martinavičius, A.; Danoix, R.; Drouet, M.; Templier, C.; Hannoyer, B.; Danoix, F. Atom probe tomography characterization of nitrogen induced decomposition in low temperature plasma nitrided 304L austenitic stainless steel. *Mater. Lett.* **2015**, *139*, 153–156. [[CrossRef](#)]
203. Sasidhar, K.N.; Meka, S.R. Thermodynamic reasoning for colossal N supersaturation in austenitic and ferritic stainless steels during low-temperature nitridation. *Sci. Rep.* **2019**, *9*, 7996. [[CrossRef](#)]
204. Che, H.L.; Tong, S.; Wang, K.S.; Lei, M.K.; Somers, M.A.J. Co-existence of γ_N' phase and γ_N phase on nitrided austenitic Fe–Cr–Ni alloys- I. experiment. *Acta Mater.* **2019**, *177*, 35–45. [[CrossRef](#)]
205. Che, H.L.; Lei, M.K.; Somers, M.A.J. A simple model for nitrogen-induced lattice expansion of γ_N' and γ_N phases in Fe–Cr–Ni alloys with different chromium contents. *Philos. Mag. Lett.* **2020**, *100*, 435–441. [[CrossRef](#)]
206. Hummelshøj, T.S.; Christiansen, T.L.; Somers, M.A.J. Lattice expansion of carbon-stabilized expanded austenite. *Scr. Mater.* **2010**, *63*, 761–763. [[CrossRef](#)]
207. Oddershede, J.; Christiansen, T.L.; Ståhl, K.; Somers, M.A.J. Extended X-ray absorption fine structure investigation of nitrogen stabilized expanded austenite. *Scr. Mater.* **2010**, *62*, 290–293. [[CrossRef](#)]
208. Oddershede, J.; Christiansen, T.L.; Ståhl, K.; Somers, M.A.J. Extended X-ray absorption fine structure investigation of carbon stabilized expanded austenite and carbides in stainless steel AISI 316. *Steel Res. Int.* **2011**, *82*, 1248–1254. [[CrossRef](#)]
209. Brink, B.K.; Ståhl, K.; Christiansen, T.L.; Frandsen, C.; Hansen, M.F.; Somers, M.A.J. Composition-dependent variation of magnetic properties and interstitial ordering in homogeneous expanded austenite. *Acta Mater.* **2016**, *106*, 32–39. [[CrossRef](#)]
210. Che, H.L.; Lei, M.K. Microstructure of perfect nitrogen-expanded austenite formed by unconstrained nitriding. *Scr. Mater.* **2021**, *194*, 113705. [[CrossRef](#)]
211. Kappaganthu, S.R.; Sun, Y. Formation of an MN-type cubic nitride phase in reactively sputtered stainless steel-nitrogen films. *J. Cryst. Growth* **2004**, *267*, 385–393. [[CrossRef](#)]
212. Fossati, A.; Borgioli, F.; Galvanetto, E.; Bacci, T. Glow-discharge nitriding of AISI 316L austenitic stainless steel: Influence of treatment time. *Surf. Coat. Technol.* **2006**, *200*, 3511–3517. [[CrossRef](#)]
213. Thaiwatthana, S.; Li, X.Y.; Dong, H.; Bell, T. Comparison studies on properties of nitrogen and carbon S phase on low temperature plasma alloyed AISI 316 stainless steel. *Surf. Eng.* **2002**, *18*, 433–437. [[CrossRef](#)]
214. Sun, Y.; Li, X.; Bell, T. Low temperature plasma carburising of austenitic stainless steels for improved wear and corrosion resistance. *Surf. Eng.* **1999**, *15*, 49–54. [[CrossRef](#)]
215. Duarte, M.C.S.; Godoy, C.; Wilson, J.C.A.-B. Analysis of sliding wear tests of plasma processed AISI 316L steel. *Surf. Coat. Technol.* **2014**, *260*, 316–325. [[CrossRef](#)]
216. Sun, Y.; Bell, T. Sliding wear characteristics of low temperature plasma nitrided 316 austenitic stainless steel. *Wear* **1998**, *218*, 34–42. [[CrossRef](#)]
217. Baranowska, J.; Franklin, S.E.; Kochmańska, A. Wear behaviour of low-temperature gas nitrided austenitic stainless steel in a corrosive liquid environment. *Wear* **2007**, *263*, 669–673. [[CrossRef](#)]
218. Ceschini, L.; Chiavari, C.; Marconi, A.; Martini, C. Influence of the countermaterial on the dry sliding friction and wear behaviour of low temperature carburized AISI 316L steel. *Tribol. Int.* **2013**, *67*, 36–43. [[CrossRef](#)]
219. De Las Heras, E.; Santamaría, D.G.; García-Luis, A.; Cabo, A.; Brizuela, M.; Ybarra, G.; Mingolo, N.; Brühl, S.; Corengia, P. Microstructure and Wear Behavior of DC-Pulsed Plasma Nitrided AISI 316L Austenitic Stainless Steel. *Plasma Process. Polym.* **2007**, *4*, S741–S745. [[CrossRef](#)]
220. Zhu, X.M.; Lei, M.K. Pitting corrosion resistance of high nitrogen f.c.c. phase in plasma source ion nitrided austenitic stainless steel. *Surf. Coat. Technol.* **2000**, *131*, 400–403. [[CrossRef](#)]
221. Fossati, A.; Borgioli, F.; Galvanetto, E.; Bacci, T. Corrosion resistance properties of glow-discharge nitrided AISI 316L austenitic stainless steel in NaCl solutions. *Corros. Sci.* **2006**, *48*, 1513–1527. [[CrossRef](#)]
222. Flis-Kabulska, I.; Sun, Y.; Flis, J. Monitoring the near-surface pH to probe the role of nitrogen in corrosion behaviour of low-temperature plasma nitrided 316L stainless steel. *Electrochim. Acta* **2013**, *104*, 208–215. [[CrossRef](#)]
223. Abreu, C.M.; Cristóbal, M.J.; Merino, P.; Nóvoa, X.R.; Pena, G.; Pérez, M.C. Electrochemical behaviour of an AISI 304L stainless steel implanted with nitrogen. *Electrochim. Acta* **2008**, *53*, 6000–6007. [[CrossRef](#)]
224. Zhu, X.M.; Guo, Y.; Xing, Z.Q.; Lei, M.K. Effect of Nitrogen on Semiconducting Properties of Passive Films of a High Nitrogen Face-Centered-Cubic Phase Formed on Austenitic Stainless Steel. *J. Electrochem. Soc.* **2012**, *159*, C319–C325. [[CrossRef](#)]
225. Li, C.X.; Bell, T. Corrosion properties of active screen plasma nitrided 316 austenitic stainless steel. *Corros. Sci.* **2004**, *46*, 1527–1547. [[CrossRef](#)]
226. Buhagiar, J.; Dong, H. Corrosion properties of S-phase layers formed on medical grade austenitic stainless steel. *J. Mater. Sci. Mater. Med.* **2012**, *23*, 271–281. [[CrossRef](#)]

227. Stio, M.; Martinesi, M.; Treves, C.; Borgioli, F. Cultures and co-cultures of human blood mononuclear cells and endothelial cells for the biocompatibility assessment of surface modified AISI 316L austenitic stainless steel. *Mater. Sci. Eng. C* **2016**, *69*, 1081–1091. [[CrossRef](#)]
228. Lei, M.K.; Zhang, Z.L.; Zhu, X.M. Effects of nitrogen-induced hcp martensite formation on corrosion resistance of plasma source ion nitrided austenitic stainless steel. *J. Mater. Sci. Lett.* **1999**, *18*, 1537–1538. [[CrossRef](#)]
229. Gontijo, L.C.; Machado, R.; Kuri, S.E.; Casteletti, L.C.; Nascente, P.A.P. Corrosion resistance of the layers formed on the surface of plasma-nitrided AISI 304L steel. *Thin Solid Films* **2006**, *515*, 1093–1096. [[CrossRef](#)]